

The Supersymmetric Parameter Space in Light of *B*-physics Observables and Electroweak Precision Data

J. Ellis¹, S. Heinemeyer², K.A. Olive³, A.M. Weber⁴ and G. Weiglein⁵

¹*TH Division, Physics Department, CERN, Geneva, Switzerland*

²*Instituto de Fisica de Cantabria (CSIC-UC), Santander, Spain*

³*William I. Fine Theoretical Physics Institute,
University of Minnesota, Minneapolis, MN 55455, USA*

⁴*Max-Planck-Institut für Physik, Föhringer Ring 6, D-80805 Munich, Germany*

⁵*IPPP, University of Durham, Durham DH1 3LE, UK*

Abstract

Indirect information about the possible scale of supersymmetry (SUSY) breaking is provided by *B*-physics observables (BPO) as well as electroweak precision observables (EWPO). We combine the constraints imposed by recent measurements of the BPO $\text{BR}(b \rightarrow s\gamma)$, $\text{BR}(B_s \rightarrow \mu^+\mu^-)$, $\text{BR}(B_u \rightarrow \tau\nu_\tau)$ and ΔM_{B_s} with those obtained from the experimental measurements of the EWPO M_W , $\sin^2\theta_{\text{eff}}$, Γ_Z , $(g-2)_\mu$ and M_h , incorporating the latest theoretical calculations of these observables within the Standard Model and supersymmetric extensions. We perform a χ^2 fit to the parameters of the constrained minimal supersymmetric extension of the Standard Model (CMSSM), in which the SUSY-breaking parameters are universal at the GUT scale, and the non-universal Higgs model (NUHM), in which this constraint is relaxed for the soft SUSY-breaking contributions to the Higgs masses. Assuming that the lightest supersymmetric particle (LSP) provides the cold dark matter density preferred by WMAP and other cosmological data, we scan over the remaining parameter space. Within the CMSSM, we confirm the preference found previously for a relatively low SUSY-breaking scale, though there is some slight tension between the EWPO and the BPO. In studies of some specific NUHM scenarios compatible with the cold dark matter constraint we investigate $(M_A, \tan\beta)$ planes and find preferred regions that have values of χ^2 somewhat lower than in the CMSSM.

February 1, 2008

1 Introduction

The dimensionality of the parameter space of the minimal supersymmetric extension of the Standard Model (MSSM) [1, 2] is so high that phenomenological analyses often make simplifying assumptions that reduce drastically the number of parameters. One assumption that is frequently employed is that (at least some of) the soft SUSY-breaking parameters are universal at some high input scale, before renormalization. One model based on this simplification is the constrained MSSM (CMSSM), in which all the soft SUSY-breaking scalar masses m_0 are assumed to be universal at the GUT scale, as are the soft SUSY-breaking gaugino masses $m_{1/2}$ and trilinear couplings A_0 . The assumption that squarks and sleptons with the same gauge quantum numbers have the same masses is motivated by the absence of identified supersymmetric contributions to flavour-changing neutral interactions and rare decays (see Ref. [3] and references therein). Universality between squarks and sleptons with different gauge interactions may be motivated by some GUT scenarios [4]. However, the universality of the soft SUSY-breaking contributions to the Higgs scalar masses is less motivated, and is relaxed in the non-universal Higgs model (NUHM) [5–7].

There are different possible approaches to analyzing the reduced parameter spaces of the CMSSM and the NUHM. One minimal approach would be to approximate the various theoretical, phenomenological, experimental, astrophysical and cosmological constraints naively by θ functions, determine the domains of the SUSY parameters allowed by their combination, and not attempt to estimate which values of the parameters might be more or less likely. This approach would perhaps be adequate if one were agnostic about the existence of low-energy SUSY. On the other hand, if one were more positive about its existence, and keen to find which SUSY parameter values were more ‘probable’, one would make a likelihood analysis and take seriously any possible hints that the Standard Model (SM) might not fit perfectly the available data. This is the approach taken in this paper. We perform a combined χ^2 analysis of electroweak precision observables (EWPO), going beyond previous such analyses [8, 9] (see also Ref. [10]), and of B -physics observables (BPO), including some that have not been included before in comprehensive analyses of the SUSY parameter space (see, however, Ref. [11]). In the past, the set of EWPO included in such analyses have been the W boson mass M_W , the effective leptonic weak mixing angle $\sin^2 \theta_{\text{eff}}$, the anomalous magnetic moment of the muon $(g - 2)_\mu$, and the mass of the lightest MSSM Higgs boson mass M_h . Since our previous study, the theoretical link between experimental observables and $\sin^2 \theta_{\text{eff}}$ within the Standard Model has become more precise, changing the χ^2 distribution for the possible MSSM contribution. We also include in this analysis a new EWPO, namely

the total Z boson width Γ_Z . In addition, we now include four BPO: the branching ratios $\text{BR}(b \rightarrow s\gamma)$, $\text{BR}(B_s \rightarrow \mu^+\mu^-)$ and $\text{BR}(B_u \rightarrow \tau\nu_\tau)$, and the B_s mass mixing parameter ΔM_{B_s} . For each observable, we construct the χ^2 function including both theoretical and experimental systematic uncertainties, as well as statistical errors. The largest theoretical systematic uncertainty is that in $\text{BR}(b \rightarrow s\gamma)$, mainly associated with the renormalization-scale ambiguity. Since this is not a Gaussian error, we do not add it in quadrature with the other errors. Instead, in order to be conservative, we prefer to add it linearly.

For our CMSSM analysis, the fact that the cold dark matter density is known from astrophysics and cosmology with an uncertainty smaller than 10 % fixes with proportional precision one combination of the SUSY parameters, enabling us to analyze the overall χ^2 value as a function of $m_{1/2}$ for fixed values of $\tan\beta$ and A_0 . The value of $|\mu|$ is fixed by the electroweak vacuum conditions, the value of m_0 is fixed with a small error by the dark matter density, and the Higgs mass parameters are fixed by the universality assumption. As in previous analyses, we consider various representative values of $A_0 \propto m_{1/2}$ for the specific choices $\tan\beta = 10, 50$. Also as previously, we find a marked preference for relatively small values of $m_{1/2} \sim 300, 600$ GeV for $\tan\beta = 10, 50$, respectively, driven largely by $(g-2)_\mu$ with some assistance from M_W . This preference would have been more marked if the BPO were not taken into account. Indeed, there is a slight tension between the EWPO and the BPO, with the latter disfavouring smaller $m_{1/2}$, particularly for large $\tan\beta$. As corollaries of this analysis, we present the χ^2 distributions for the masses of various MSSM particles, including the lightest Higgs boson mass M_h . This shows a strong preference for $M_h \sim 115$ GeV, allowing M_h as high as 120 GeV with $\Delta\chi^2 \sim 4$.

In view of the slight tension between the EWPO and BPO within the CMSSM, we have gone on to explore the NUHM, which effectively has M_A and μ as additional free parameters as compared to the CMSSM. In particular, we have investigated whether the NUHM reconciles more easily the EWPO and BPO, and specifically whether there exist NUHM points with significantly lower χ^2 . As pointed out previously, generic NUHM parameter planes in which the other variables are held fixed do not satisfy the cold dark matter density constraint imposed by WMAP et al. In this paper, we introduce ‘WMAP surfaces’, which are $(M_A, \tan\beta)$ planes across in which the other variables are adjusted continuously so as to maintain the LSP density within the WMAP range. We then examine the χ^2 values of the EWPO and BPO in the NUHM as functions over these WMAP surfaces ¹. In each of the

¹A more complete characterization of these WMAP surfaces will be given elsewhere [12], as well as a discussion of their possible use as ‘benchmark scenarios’ for evaluating the prospects for MSSM Higgs phenomenology at the Tevatron, the LHC and elsewhere.

WMAP surfaces we find localized regions preferred by the EWPO and BPO and, in some cases, the minimum value of χ^2 is significantly lower than along the WMAP strips in the CMSSM, indicating that the NUHM may help resolve the slight tension between the EWPO and the BPO. We explore this possibility further by investigating lines that explore further the NUHM parameter space in neighbourhoods of the low- χ^2 points in the WMAP surfaces.

In Sect. 2 we review the current status of the EWPO and BPO that we use, our treatment of the available theoretical calculations and their errors, as well as their present experimental values. The analysis within the CMSSM can be found in Sect. 3, while the NUHM investigation is presented in Sect. 4. Sect. 5 summarizes our principal conclusions.

2 Current Experimental Data

The relevant data set includes five EWPO: the mass of the W boson, M_W , the effective leptonic weak mixing angle, $\sin^2 \theta_{\text{eff}}$, the total Z boson width, Γ_Z , the anomalous magnetic moment of the muon, $(g-2)_\mu$, and the mass of the lightest MSSM Higgs boson, M_h . In addition, we include four BPO: the branching ratios $\text{BR}(b \rightarrow s\gamma)$, $\text{BR}(B_s \rightarrow \mu^+ \mu^-)$, and $\text{BR}(B_u \rightarrow \tau \nu_\tau)$ as well as the B_s mass-mixing parameter ΔM_{B_s} . A detailed description of the EWPO and $\text{BR}(b \rightarrow s\gamma)$ can be found in Refs. [8, 9, 13, 14].

In this Section we start our analysis by recalling the current precisions of the experimental results and the theoretical predictions for all these observables. We also display the CMSSM predictions for the EWPO (where new results are available), and also for the BPO. These predictions serve as examples of the expected ranges of the EWPO and BPO values once SUSY corrections are taken into account.

In the following, we refer to the theoretical uncertainties from unknown higher-order corrections as ‘intrinsic’ theoretical uncertainties and to the uncertainties induced by the experimental errors of the SM input parameters as ‘parametric’ theoretical uncertainties. We do not discuss here the theoretical uncertainties in the renormalization-group running between the high-scale input parameters and the weak scale, see Ref. [15] for a recent discussion in the context of calculations of the cold dark matter (CDM) density. At present, these uncertainties are less important than the experimental and theoretical uncertainties in the precision observables.

Assuming that the nine observables listed above are uncorrelated, a χ^2 fit has been performed with

$$\chi^2 \equiv \sum_{n=1}^7 \left[\left(\frac{R_n^{\text{exp}} - R_n^{\text{theo}}}{\sigma_n} \right)^2 + 2 \log \left(\frac{\sigma_n}{\sigma_n^{\text{min}}} \right) \right] + \chi_{M_h}^2 + \chi_{B_s}^2. \quad (1)$$

Here R_n^{exp} denotes the experimental central value of the n th observable (M_W , $\sin^2 \theta_{\text{eff}}$, Γ_Z , $(g-2)_\mu$ and $\text{BR}(b \rightarrow s\gamma)$, $\text{BR}(B_u \rightarrow \tau\nu_\tau)$, ΔM_{B_s}), R_n^{theo} is the corresponding MSSM prediction and σ_n denotes the combined error, as specified below. Additionally, σ_n^{min} is the minimum combined error over the parameter space of each data set as explained below, and $\chi_{M_h}^2$ and $\chi_{B_s}^2$ denote the χ^2 contribution coming from the experimental limits on the lightest MSSM Higgs boson mass and on $\text{BR}(B_s \rightarrow \mu^+\mu^-)$, respectively, which are also described below.

We also list below the parametric uncertainties in the predictions on the observables induced by the experimental uncertainty in the top- and bottom-quark masses. These errors neglect, however, the effects of varying m_t and m_b on the SUSY spectrum that are induced via the RGE running. In order to take the m_t and m_b parametric uncertainties correctly into account, we evaluate the SUSY spectrum and the observables for each data point first for the nominal values $m_t = 171.4$ GeV [16]² and $m_b(m_b) = 4.25$ GeV, then for $m_t = (171.4 + 1.0)$ GeV and $m_b(m_b) = 4.25$ GeV, and finally for $m_t = 171.4$ GeV and $m_b(m_b) = (4.25 + 0.1)$ GeV. The latter two evaluations are used by appropriate rescaling to estimate the full parametric uncertainties induced by the experimental uncertainties $\delta m_t^{\text{exp}} = 2.1$ GeV [16]³ and $\delta m_b(m_b)^{\text{exp}} = 0.11$ GeV. These parametric uncertainties are then added to the other errors (intrinsic, parametric, and experimental) of the observables as described in the text below.

We preface our discussion by describing our treatment of the cosmological cold dark matter density, which guides our subsequent analysis of the EWPO and BPO within the CMSSM and NUHM.

2.1 Cold Dark Matter Density

Throughout this analysis, we focus our attention on parameter points that yield the correct value of the cold dark matter density inferred from WMAP and other data, namely $0.094 < \Omega_{\text{CDM}} h^2 < 0.129$ [18]. The fact that the density is relatively well known restricts the SUSY parameter space to a thin, fuzzy ‘WMAP hypersurface’, effectively reducing its

²Using the most recent experimental value, $m_t = 170.9$ GeV [17] would have a minor impact on our analysis.

³Using the most recent experimental m_t error of 1.8 GeV [17] would also have a minor impact on our analysis.

dimensionality by one. The variations in the EWPO and BPO across this hypersurface may in general be neglected, so that we may treat the cold dark matter constraint effectively as a δ function. For example, in the CMSSM we focus our attention on ‘WMAP lines’ in the $(m_{1/2}, m_0)$ planes for discrete values of the other SUSY parameters $\tan\beta$ and A_0 [19, 20]. Correspondingly, in the following, for each value of $m_{1/2}$, we present theoretical values for the EWPO and BPO corresponding to the values of m_0 on WMAP strips.

We note, however, that for any given value of $m_{1/2}$ there may be more than one value of m_0 that yields a cold dark matter density within the allowed range, implying that there may be more than one WMAP line traversing the $(m_{1/2}, m_0)$ plane. Specifically, in the CMSSM there is, in general, one WMAP line in the coannihilation/rapid-annihilation funnel region and another in the focus-point region, at higher m_0 . Consequently, each EWPO and BPO may have more than one value for any given value of $m_{1/2}$. In the following, we restrict our study of the upper WMAP line to the part with $m_0 < 2000$ GeV for $\tan\beta = 10$ and $m_0 < 3000$ GeV for $\tan\beta = 50$, restricting in turn the range of $m_{1/2}$.

The NUHM, with M_A and μ , has two more parameters than the CMSSM, which characterize the degrees of non-universality of the two Higgs masses. The WMAP lines therefore should, in principle, be generalized to three-volumes in the higher-dimensional NUHM parameter space where the cold dark matter density remains within the WMAP range. We prefer here to focus our attention on ‘WMAP surfaces’ that are slices through these three-volumes with specific fixed values for (combinations of) the other NUHM parameters. These WMAP surfaces are introduced in more detail in the subsequent section describing our NUHM analysis, and will be discussed in more detail in Ref. [12].

In regions that depend sensitively on the input values of m_t and $m_b(m_b)$, such as the focus-point region [21] in the CMSSM, the corresponding parametric uncertainty can become very large. In essence, the ‘WMAP hypersurface’ moves significantly as m_t varies (and to a lesser extent also $m_b(m_b)$), but remains thin. Incorporating this large parametric uncertainty naively in eq. (1) would artificially suppress the overall χ^2 value for such points. This artificial suppression is avoided by adding the second term in eq. (1), where σ_n^{\min} is the value of the combined error evaluated for parameter choices which minimize χ_n^2 over the full data set.

2.2 The W Boson Mass

The W boson mass can be evaluated from

$$M_W^2 \left(1 - \frac{M_W^2}{M_Z^2} \right) = \frac{\pi\alpha}{\sqrt{2}G_F} (1 + \Delta r), \quad (2)$$

where α is the fine structure constant and G_F the Fermi constant. The radiative corrections are summarized in the quantity Δr [22]. The prediction for M_W within the SM or the MSSM is obtained by evaluating Δr in these models and solving eq. (2) for M_W .

We use the most precise available result for M_W in the MSSM [23]. Besides the full SM result, for the MSSM it includes the full set of one-loop contributions [23–25] as well as the corrections of $\mathcal{O}(\alpha\alpha_s)$ [26] and of $\mathcal{O}(\alpha_{t,b}^2)$ [27, 28] to the quantity $\Delta\rho$; see Ref. [23] for details.

The remaining intrinsic theoretical uncertainty in the prediction for M_W within the MSSM is still significantly larger than in the SM. For realistic parameters it has been estimated as [28]

$$\Delta M_W^{\text{intr,current}} \lesssim 10 \text{ MeV} , \quad (3)$$

depending on the mass scale of the supersymmetric particles. The parametric uncertainties are dominated by the experimental error of the top-quark mass and the hadronic contribution to the shift in the fine structure constant. Their current errors induce the following parametric uncertainties [14]

$$\delta m_t^{\text{current}} = 2.1 \text{ GeV} \Rightarrow \Delta M_W^{\text{para},m_t,\text{current}} \approx 13 \text{ MeV}, \quad (4)$$

$$\delta(\Delta\alpha_{\text{had}}^{\text{current}}) = 35 \times 10^{-5} \Rightarrow \Delta M_W^{\text{para},\Delta\alpha_{\text{had}},\text{current}} \approx 6.3 \text{ MeV} . \quad (5)$$

The present experimental value of M_W is [29–33]

$$M_W^{\text{exp,current}} = 80.398 \pm 0.025 \text{ GeV}. \quad (6)$$

We add the experimental and theoretical errors for M_W in quadrature in our analysis.

The current status of the MSSM prediction and the experimental resolution is shown in Fig. 1. We note that the CMSSM predictions for M_W in the coannihilation and focus-point regions are quite similar, and depend little on A_0 . We also see that small values of $m_{1/2}$ are slightly preferred, reflecting the familiar fact that the experimental value of M_W is currently somewhat higher than the SM prediction.

2.3 The Effective Leptonic Weak Mixing Angle

The effective leptonic weak mixing angle at the Z boson peak can be written as

$$\sin^2 \theta_{\text{eff}} = \frac{1}{4} \left(1 - \text{Re} \frac{v_{\text{eff}}}{a_{\text{eff}}} \right) , \quad (7)$$

where v_{eff} and a_{eff} denote the effective vector and axial couplings of the Z boson to charged leptons. We use the most precise available result for $\sin^2 \theta_{\text{eff}}$ in the MSSM [14]. The prediction contains the same classes of higher-order corrections as described in Sect. 2.2.

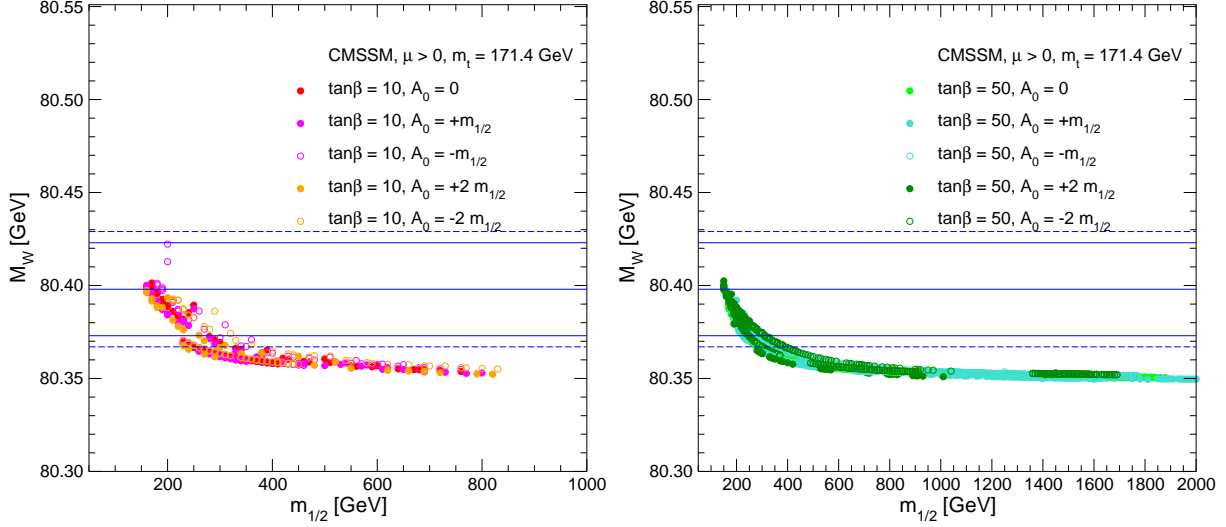


Figure 1: The CMSSM predictions for M_W are shown as functions of $m_{1/2}$ along the WMAP strips for (a) $\tan\beta = 10$ and (b) $\tan\beta = 50$ for various A_0 values. In each panel, the centre (solid) line is the present central experimental value, and the (solid) outer lines show the current $\pm 1\text{-}\sigma$ range. The dashed lines correspond to the full error including also parametric and intrinsic uncertainties.

In the MSSM with real parameters, the remaining intrinsic theoretical uncertainty in the prediction for $\sin^2\theta_{\text{eff}}$ has been estimated as [28]

$$\Delta \sin^2\theta_{\text{eff}}^{\text{intr,current}} \lesssim 7 \times 10^{-5}, \quad (8)$$

depending on the SUSY mass scale. The current experimental errors of m_t and $\Delta\alpha_{\text{had}}$ induce the following parametric uncertainties [14]

$$\delta m_t^{\text{current}} = 2.1 \text{ GeV} \Rightarrow \Delta \sin^2\theta_{\text{eff}}^{\text{para},m_t,\text{current}} \approx 6.3 \times 10^{-5}, \quad (9)$$

$$\delta(\Delta\alpha_{\text{had}}^{\text{current}}) = 35 \times 10^{-5} \Rightarrow \Delta \sin^2\theta_{\text{eff}}^{\text{para},\Delta\alpha_{\text{had}},\text{current}} \approx 12 \times 10^{-5}. \quad (10)$$

The experimental value is [29, 30]

$$\sin^2\theta_{\text{eff}}^{\text{exp,current}} = 0.23153 \pm 0.00016. \quad (11)$$

We add the experimental and theoretical errors for $\sin^2\theta_{\text{eff}}$ in quadrature in our analysis.

As compared with our older analyses [8, 9] we now use a new result for $\sin^2\theta_{\text{eff}}$, obtained recently, that differs non-negligibly from that used previously, due to the inclusion of more higher-order corrections (which also result in a smaller intrinsic error). The corresponding new results in the CMSSM are shown in Fig. 2 for $\tan\beta = 10$ (left) and $\tan\beta = 50$ (right) as

functions of $m_{1/2}$. Whereas previously the agreement with the experimental result was best for $m_{1/2} \approx 300$ GeV, we now find best agreement for large $m_{1/2}$ values. However, taking all uncertainties into account, the deviation for $m_{1/2}$ generally stays below the level of one sigma. We note that the predictions for $\sin^2 \theta_{\text{eff}}$ in the coannihilation and focus-point regions are somewhat different.

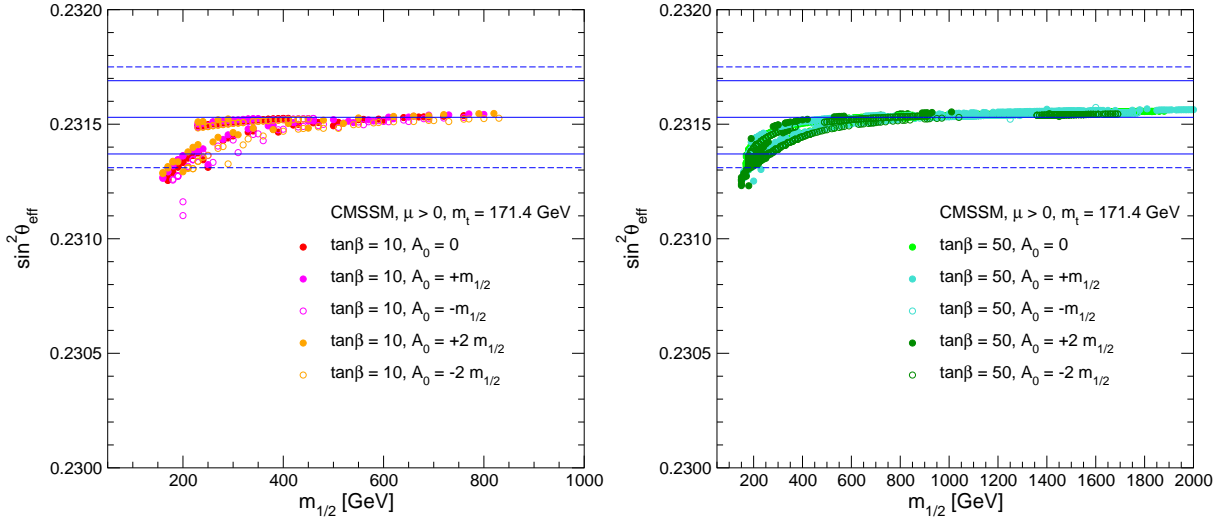


Figure 2: The CMSSM predictions for $\sin^2 \theta_{\text{eff}}$ as functions of $m_{1/2}$ along the WMAP strips for (a) $\tan \beta = 10$ and (b) $\tan \beta = 50$ for various A_0 values. In each panel, the centre (solid) line is the present central experimental value, and the (solid) outer lines show the current $\pm 1\sigma$ range. The dashed lines correspond to the full error including also parametric and intrinsic uncertainties.

2.4 The Total Z Boson Decay Width

The total Z boson decay width, Γ_Z , is given by

$$\Gamma_Z = \Gamma_l + \Gamma_h + \Gamma_{\tilde{\chi}_1^0}, \quad (12)$$

where $\Gamma_{l,h}$ are the rates for decays into SM leptons and quarks, respectively, and $\Gamma_{\tilde{\chi}_1^0}$ denotes the decay width to the lightest neutralino. We have checked that, for the parameters analyzed in this paper, always $\Gamma_{\tilde{\chi}_1^0} = 0$. However, SUSY particles enter via virtual corrections to Γ_l and Γ_h . We use the most precise available result for Γ_Z in the MSSM [14]. The prediction contains the same classes of MSSM higher-order corrections as described in Sect. 2.2.

So far no estimate has been made of the intrinsic uncertainty in the prediction for Γ_Z in the MSSM. Following the numerical analysis in Ref. [14], we use a conservative value of

$$\Delta\Gamma_Z^{\text{intr,current}} \lesssim 1.0 \text{ MeV} \quad (13)$$

The current experimental errors of m_t and $\Delta\alpha_{\text{had}}$ induce the following parametric uncertainties [14]

$$\delta m_t^{\text{current}} = 2.1 \text{ GeV} \Rightarrow \Delta\Gamma_Z^{\text{para},m_t,\text{current}} \approx 0.51 \text{ MeV}, \quad (14)$$

$$\delta(\Delta\alpha_{\text{had}}^{\text{current}}) = 35 \times 10^{-5} \Rightarrow \Delta\Gamma_Z^{\text{para},\Delta\alpha_{\text{had}},\text{current}} \approx 0.32 \text{ MeV}. \quad (15)$$

The experimental value is [29, 30]

$$\Gamma_Z^{\text{exp,current}} = 2495.2 \pm 2.3 \text{ MeV}. \quad (16)$$

We add the experimental and theoretical errors for Γ_Z in quadrature in our analysis.

A comparison of the MSSM prediction with the experimental value is shown in Fig. 3. We see that the experimental value is within $\sim 1/2$ a standard deviation of the CMSSM value at large $m_{1/2}$, which corresponds to the SM value with the same Higgs boson mass. The marginal improvement in the CMSSM prediction at small $m_{1/2}$ is not significant. We note that the predictions for Γ_Z in the coannihilation and focus-point regions are somewhat different.

2.5 The Anomalous Magnetic Moment of the Muon

The SM prediction for the anomalous magnetic moment of the muon (see Refs. [34–38] for reviews) depends on the evaluation of QED contributions (see Refs. [39, 40] for recent updates), the hadronic vacuum polarization and light-by-light (LBL) contributions. The former have been evaluated in Refs. [38, 41–46] and the latter in Refs. [47–51]. The evaluations of the hadronic vacuum polarization contributions using e^+e^- and τ decay data give somewhat different results. In view of the fact that recent e^+e^- measurements tend to confirm earlier results, whereas the correspondence between previous τ data and preliminary data from BELLE is not so clear, and also in view of the additional uncertainties associated with the isospin transformation from τ decay, we use here the latest estimate based on e^+e^- data [46]:

$$a_\mu^{\text{theo}} = (11\,659\,180.5 \pm 4.4_{\text{had}} \pm 3.5_{\text{LBL}} \pm 0.2_{\text{QED+EW}}) \times 10^{-10}, \quad (17)$$

where the source of each error is labeled. We note that the new e^+e^- data sets that have recently been published in Refs. [52–54] have been partially included in the updated estimate of $(g-2)_\mu$.

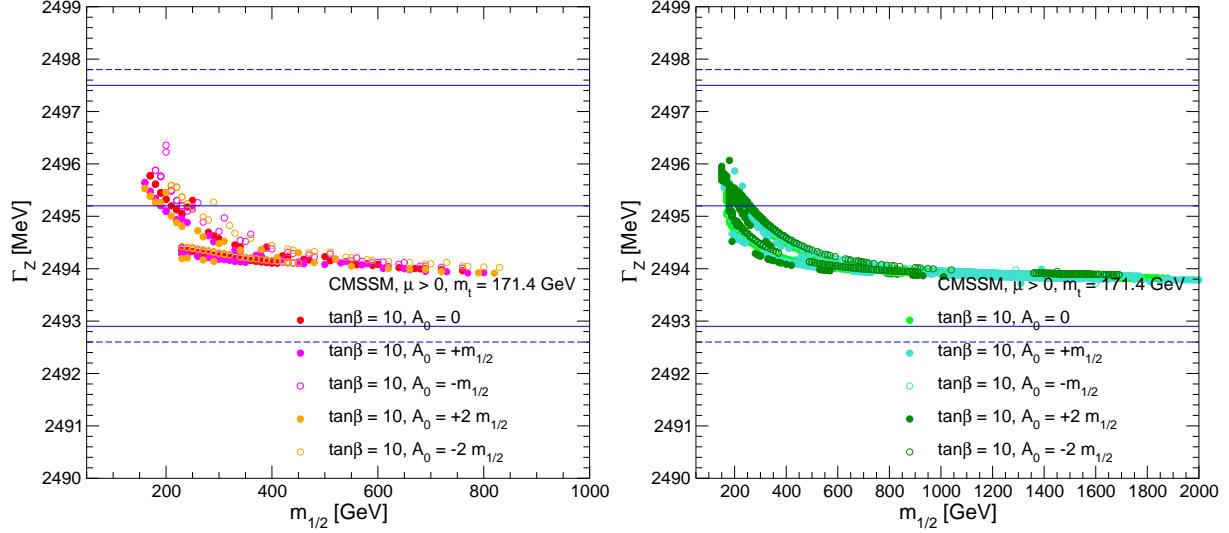


Figure 3: The CMSSM predictions for Γ_Z as functions of $m_{1/2}$ along the WMAP strips for (a) $\tan\beta = 10$ and (b) $\tan\beta = 50$ for various A_0 values. In each panel, the centre (solid) line is the present central experimental value, and the (solid) outer lines show the current $\pm 1\text{-}\sigma$ range. The dashed lines correspond to the full error including also parametric and intrinsic uncertainties.

The SM prediction is to be compared with the final result of the Brookhaven $(g-2)_\mu$ experiment E821 [55, 56], namely:

$$a_\mu^{\text{exp}} = (11\,659\,208.0 \pm 6.3) \times 10^{-10}, \quad (18)$$

leading to an estimated discrepancy [46, 57]

$$a_\mu^{\text{exp}} - a_\mu^{\text{theo}} = (27.5 \pm 8.4) \times 10^{-10}, \quad (19)$$

equivalent to a $3.3\text{-}\sigma$ effect⁴. While it would be premature to regard this deviation as a firm evidence for new physics, within the context of SUSY, it does indicate a preference for a non-zero contribution.

Concerning the MSSM contribution, the complete one-loop result was evaluated a decade ago [58]. In view of the correlation between the signs of $(g-2)_\mu$ and of μ [59], variants of the MSSM with $\mu < 0$ are already severely challenged by the present data on a_μ , whether one uses either the e^+e^- or τ decay data, so we restrict our attention in this paper to models with $\mu > 0$. In addition to the full one-loop contributions, the leading QED two-loop corrections

⁴Three other recent evaluations yield slightly different numbers [37, 38, 43], but similar discrepancies with the SM prediction.

have also been evaluated [60]. Further corrections at the two-loop level have been obtained recently [61, 62], leading to corrections to the one-loop result that are $\lesssim 10\%$. These corrections are taken into account in our analysis according to the approximate formulae given in Refs. [61, 62].

The current status of the CMSSM prediction and the experimental resolution is shown in Fig. 4, where the 1- and 2- σ bands are shown. We note that the coannihilation and focus-point region predictions for a_μ are quite different. For $\tan\beta = 10$, the focus-point prediction agrees less well with the data, whereas for $\tan\beta = 50$ the focus-point prediction does agree well in a limited range of $m_{1/2} \sim 200$ GeV.

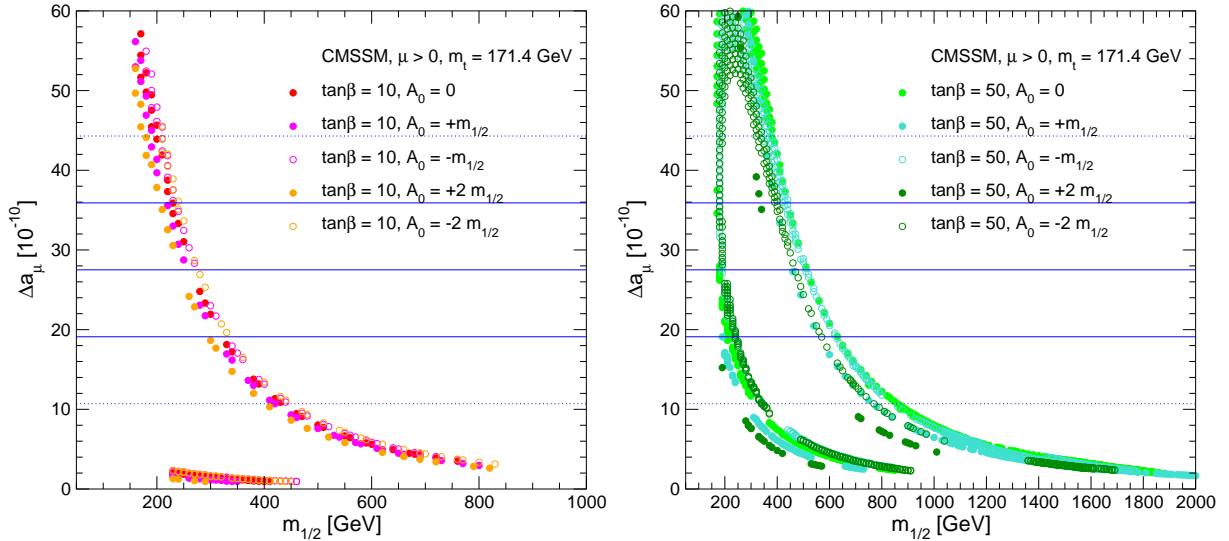


Figure 4: The CMSSM predictions for $(g - 2)_\mu$, Δa_μ , as functions of $m_{1/2}$ along the WMAP strips for (a) $\tan\beta = 10$ and (b) $\tan\beta = 50$ for various A_0 values. In each panel, the centre (solid) line is the present central experimental value, and the solid (dotted) outer lines show the current $\pm 1(2)$ - σ ranges.

2.6 The Mass of the Lightest MSSM Higgs Boson

The mass of the lightest \mathcal{CP} -even MSSM Higgs boson can be predicted in terms of the other MSSM parameters. At the tree level, the two \mathcal{CP} -even Higgs boson masses are obtained as functions of M_Z , the \mathcal{CP} -odd Higgs boson mass M_A , and $\tan\beta$, whereas other parameters enter into the loop corrections. We employ the Feynman-diagrammatic method for the theoretical prediction of M_h , using the code `FeynHiggs` [63–65], which includes all numerically relevant known higher-order corrections. The status of these results can be summarized

as follows. For the one-loop part, the complete result within the MSSM is known [66–68]. Computation of the two-loop effects is quite advanced: see Ref. [69] and references therein. These include the strong corrections at $\mathcal{O}(\alpha_t\alpha_s)$ and Yukawa corrections at $\mathcal{O}(\alpha_t^2)$ to the dominant one-loop $\mathcal{O}(\alpha_t)$ term, and the strong corrections from the bottom/sbottom sector at $\mathcal{O}(\alpha_b\alpha_s)$. In the case of the b/\tilde{b} sector corrections, an all-order resummation of the $\tan\beta$ -enhanced terms, $\mathcal{O}(\alpha_b(\alpha_s\tan\beta)^n)$, is also known [70,71]. Most recently, the $\mathcal{O}(\alpha_t\alpha_b)$ and $\mathcal{O}(\alpha_b^2)$ corrections have been derived [72]⁵. The current intrinsic error of M_h due to unknown higher-order corrections has been estimated to be [13,69,75,76]

$$\Delta M_h^{\text{intr,current}} = 3 \text{ GeV} , \quad (20)$$

which we interpret effectively as a $\sim 95\%$ confidence level limit: see below.

It should be noted that, for the unconstrained MSSM with small values of M_A and values of $\tan\beta$ which are not too small, a significant suppression of the hZZ coupling can occur compared to the SM value, in which case the experimental lower bound on M_h may be more than 20 GeV below the SM value [77]. However, we have checked that within the CMSSM and the other models studied in this paper, the hZZ coupling is always very close to the SM value. Accordingly, the bounds from the SM Higgs search at LEP [78] can be taken over directly (see e.g. Refs. [79,80]).

Concerning the χ^2 analysis, we use the complete likelihood information available from LEP. Accordingly, we evaluate as follows the M_h contribution to the overall χ^2 function⁶. Our starting points are the $CL_s(M_h)$ values provided by the final LEP results on the SM Higgs boson search, see Fig. 9 in Ref. [78]⁷. We obtain by inversion from $CL_s(M_h)$ the corresponding value of $\tilde{\chi}^2(M_h)$ determined from Ref. [81]

$$\frac{1}{2}\text{erfc}\left(\sqrt{\frac{1}{2}\tilde{\chi}^2(M_h)}\right) \equiv CL_s(M_h) , \quad (21)$$

and note the fact that $CL_s(M_h = 116.4 \text{ GeV}) = 0.5$ implies that $\tilde{\chi}^2(116.4 \text{ GeV}) = 0$ as is appropriate for a one-sided limit. Correspondingly we set $\tilde{\chi}^2(M_h > 116.4 \text{ GeV}) = 0$. The theoretical uncertainty is included by convolving the likelihood function associated with $\tilde{\chi}^2(M_h)$ and a Gaussian function, $\tilde{\Phi}_{1.5}(x)$, normalized to unity and centered around M_h , whose width is 1.5 GeV:

$$\chi^2(M_h) = -2 \log \left(\int_{-\infty}^{\infty} e^{-\tilde{\chi}^2(x)/2} \tilde{\Phi}_{1.5}(M_h - x) dx \right) . \quad (22)$$

⁵A two-loop effective potential calculation has been presented in Ref. [73], including now even the leading three-loop corrections [74], but no public code based on this result is currently available.

⁶We thank P. Bechtle and K. Desch for detailed discussions and explanations.

⁷We thank A. Read for providing us with the CL_s values.

In this way, a theoretical uncertainty of up to 3 GeV is assigned for $\sim 95\%$ of all M_h values corresponding to one parameter point. The final $\chi^2_{M_h}$ is then obtained as

$$\chi^2_{M_h} = \chi^2(M_h) - \chi^2(116.4 \text{ GeV}) \quad \text{for} \quad M_h \leq 116.4 \text{ GeV} , \quad (23)$$

$$\chi^2_{M_h} = 0 \quad \text{for} \quad M_h > 116.4 \text{ GeV} , \quad (24)$$

and is then combined with the corresponding quantities for the other observables we consider, see eq. (1).

We show in Fig. 5 the predictions for M_h in the CMSSM for $\tan\beta = 10$ (left) and $\tan\beta = 50$ (right). The predicted values of M_h are similar in the coannihilation and focus-point regions. They depend significantly on A_0 , particularly in the coannihilation region, where negative values of A_0 tend to predict very low values of M_h that are disfavoured by the LEP direct search. Also shown in Fig. 5 is the present nominal 95 % C.L. exclusion limit for a SM-like Higgs boson, namely 114.4 GeV [78], and a hypothetical LHC measurement of $M_h = 116.4 \pm 0.2$ GeV. We recall that we use the numerical value of the LEP Higgs likelihood function in our combined analysis.

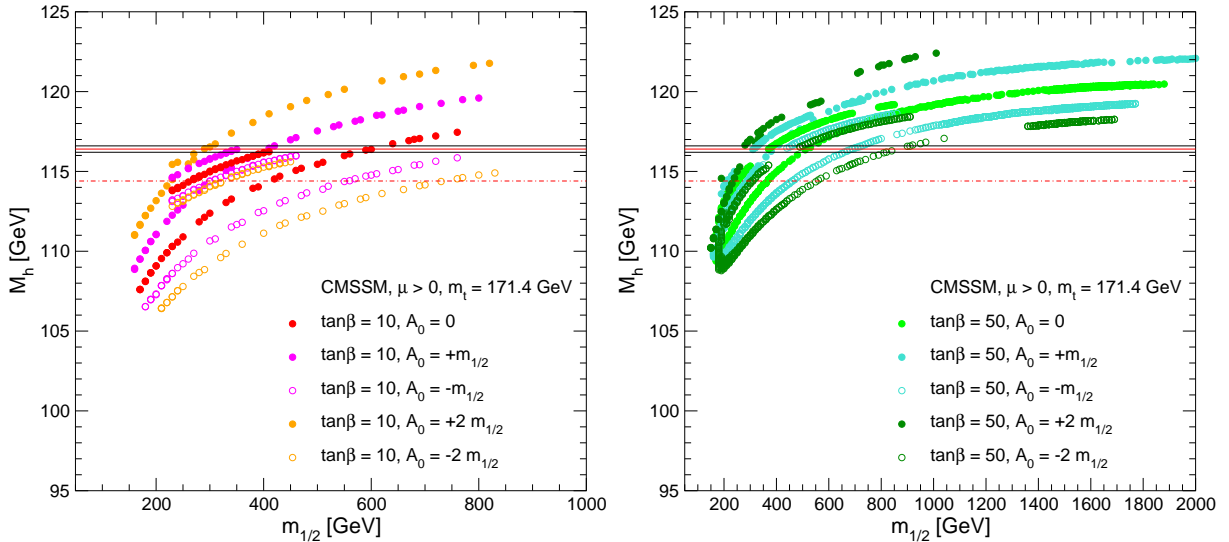


Figure 5: The CMSSM predictions for M_h as functions of $m_{1/2}$ with (a) $\tan\beta = 10$ and (b) $\tan\beta = 50$ for various A_0 . We also show the present 95% C.L. exclusion limit of 114.4 GeV and a hypothetical LHC measurement of $M_h = 116.4 \pm 0.2$ GeV.

2.7 The decay $b \rightarrow s\gamma$

Since this decay occurs at the loop level in the SM, the MSSM contribution might *a priori* be of similar magnitude. A recent theoretical estimate of the SM contribution to the branching

ratio at the NNLO QCD level is [82]

$$\text{BR}(b \rightarrow s\gamma) = (3.15 \pm 0.23) \times 10^{-4} . \quad (25)$$

We record that the error estimate for $\text{BR}(b \rightarrow s\gamma)$ is still under debate, and that other SM contributions to $b \rightarrow s\gamma$ have been calculated Refs. [83,84], but these corrections are small compared with the theoretical uncertainty quoted in (25).

For comparison, the present experimental value estimated by the Heavy Flavour Averaging Group (HFAG) is [3,85]

$$\text{BR}(b \rightarrow s\gamma) = (3.55 \pm 0.24_{-0.10}^{+0.09} \pm 0.03) \times 10^{-4}, \quad (26)$$

where the first error is the combined statistical and uncorrelated systematic uncertainty, the latter two errors are correlated systematic theoretical uncertainties and corrections respectively.

Our numerical results have been derived with the $\text{BR}(b \rightarrow s\gamma)$ evaluation provided in Refs. [86–88], incorporating also the latest SM corrections provided in Ref. [82]. The calculation has been checked against other approaches [89–91]. For the current theoretical intrinsic uncertainty of the MSSM prediction for $\text{BR}(b \rightarrow s\gamma)$ we use the SM uncertainty given in eq. (25) and add linearly the intrinsic MSSM corrections 0.15×10^{-4} [89,91] and the last two errors given by HFAG of $\simeq 0.13 \times 10^{-4}$ [3]. The full intrinsic error is then added linearly to the sum in quadrature of the experimental error given by HFAG as 0.24 and the parametric error.

In Fig. 6 we show the predictions in the CMSSM for $\text{BR}(b \rightarrow s\gamma)$ for $\tan\beta = 10, 50$ as functions of $m_{1/2}$, compared with the $1\text{-}\sigma$ experimental error (full line) and the full error (dashed line, but assuming a negligible parametric error). For $\tan\beta = 10$, we see that positive values of A_0 are disfavoured at small $m_{1/2}$, and that small values of $m_{1/2}$ are disfavoured for all the studied values of A_0 if $\tan\beta = 50$.

2.8 The Branching Ratio for $B_s \rightarrow \mu^+\mu^-$

The SM prediction for this branching ratio is $(3.4 \pm 0.5) \times 10^{-9}$ [92], and the present experimental upper limit from the Fermilab Tevatron collider is 1.0×10^{-7} at the 95% C.L. [93], providing ample room for the MSSM to dominate the SM contribution. The current Tevatron sensitivity is based on an integrated luminosity of about 780 pb^{-1} collected at CDF. The

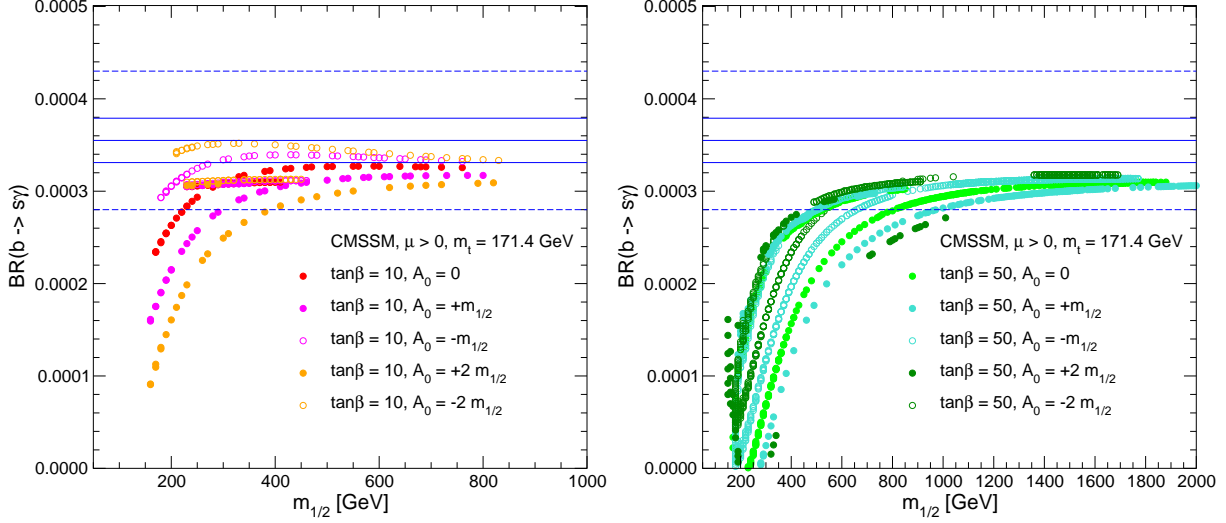


Figure 6: The CMSSM predictions for $\text{BR}(b \rightarrow s\gamma)$ as functions of $m_{1/2}$ along the WMAP strips for $\tan\beta = 10$ (left) and $\tan\beta = 50$ (right) and various choices of A_0 . The central (solid) line indicates the current experimental central value, and the other solid lines show the current $\pm 1\text{-}\sigma$ experimental range. The dashed line is the $\pm 1\text{-}\sigma$ error including also the full intrinsic error (see text).

exclusion bounds can be translated into a χ^2 function for each value of $\text{BR}(B_s \rightarrow \mu^+\mu^-)$ ⁸:

$$\tilde{\chi}^2(B_s) \equiv \chi^2(\text{BR}(B_s \rightarrow \mu^+\mu^-)) , \quad (27)$$

with $\tilde{\chi}^2(\text{BR}(B_s \rightarrow \mu^+\mu^-) < 0.266 \times 10^{-7}) = 0$. The theory uncertainty is included by convolving the likelihood function associated with $\tilde{\chi}^2(B_s)$ and a Gaussian function, $\tilde{\Phi}_{\text{th}}(x)$, normalized to unity and centered around $\text{BR}(B_s \rightarrow \mu^+\mu^-)$, whose width is given by the theory uncertainty, see below. Consequently,

$$\chi^2(B_s) = -2 \log \left(\int_{-\infty}^{\infty} e^{-\tilde{\chi}^2(x)/2} \tilde{\Phi}_{\text{th}}(\text{BR}(B_s \rightarrow \mu^+\mu^-) - x) dx \right) . \quad (28)$$

The final $\chi^2_{B_s}$ is then obtained as

$$\chi^2_{B_s} = \chi^2(B_s) - \chi^2(0.266 \times 10^{-7}) \quad \text{for} \quad \text{BR}(B_s \rightarrow \mu^+\mu^-) \geq 0.266 \times 10^{-7} , \quad (29)$$

$$\chi^2_{B_s} = 0 \quad \text{for} \quad \text{BR}(B_s \rightarrow \mu^+\mu^-) < 0.266 \times 10^{-7} . \quad (30)$$

The Tevatron sensitivity is expected to improve significantly in the future. The limit that could be reached at the end of Run II is $\sim 2 \times 10^{-8}$ assuming 8 fb^{-1} collected with each

⁸We thank C.-J. Stephen and M. Herndon for providing the χ^2 numbers. A slightly more stringent upper limit of 0.93×10^{-7} at the 95% C.L. has been announced more recently by the D0 Collaboration [94]. However, the corresponding χ^2 function is not available to us. Since the difference to the result employed here is small, we expect only a minor impact on our analysis.

detector [95]. A sensitivity even down to the SM value can be expected at the LHC. Assuming the SM value, i.e. $\text{BR}(B_s \rightarrow \mu^+ \mu^-) \approx 3.4 \times 10^{-9}$, it has been estimated [96] that LHCb can observe 33 signal events over 10 background events within 3 years of low-luminosity running. Therefore this process offers good prospects for probing the MSSM.

For the theoretical prediction we use results from Ref. [97], which are in good agreement with Ref. [98]. This calculation includes the full one-loop evaluation and the leading two-loop QCD corrections.

The theory error is estimated as follows. We take into account the parametric uncertainty induced by [99]

$$f_{B_s} = 230 \pm 30 \text{ MeV} . \quad (31)$$

The most important SUSY contribution to $\text{BR}(B_s \rightarrow \mu^+ \mu^-)$ scales as

$$\text{BR}(B_s \rightarrow \mu^+ \mu^-) \sim \frac{f_{B_s}^2}{M_A^4} . \quad (32)$$

In the models that predict the value of M_A at the low-energy scale, i.e. in our case the CMSSM, we additionally include the parametric uncertainty due to the shift in M_A in eq. (32) that is induced by the experimental errors of m_t and m_b in the RGE running [98]. These errors are added in quadrature. The intrinsic error is estimated to be negligible as compared to the parametric error. Thus the parametric error constitutes our theory error entering in eq. (28).

In Fig. 7 the CMSSM predictions for $\text{BR}(B_s \rightarrow \mu^+ \mu^-)$ for $\tan \beta = 10, 50$ as functions of $m_{1/2}$ are compared with the present Tevatron limit. For $\tan \beta = 10$ (left plot) the CMSSM prediction is significantly below the present and future Tevatron sensitivity. However, already with the current sensitivity, the Tevatron starts to probe the CMSSM coannihilation region for $\tan \beta = 50$ and $A_0 \geq 0$, whereas the CMSSM prediction in the focus-point region is significantly below the current sensitivity.

2.9 The Branching Ratio for $B_u \rightarrow \tau \nu_\tau$

The decay $B_u \rightarrow \tau \nu_\tau$ has recently been observed by BELLE [100], and the experimental world average is given by [11, 100, 101]

$$\text{BR}(B_u \rightarrow \tau \nu_\tau)_{\text{exp}} = (1.31 \pm 0.49) \times 10^{-4} . \quad (33)$$

We follow Ref. [102] for the theoretical evaluation of this decay. The main new contribution within the MSSM comes from the direct-exchange of a virtual charged Higgs boson decaying into $\tau \nu_\tau$. Taking into account the resummation of the leading $\tan \beta$ enhanced corrections,

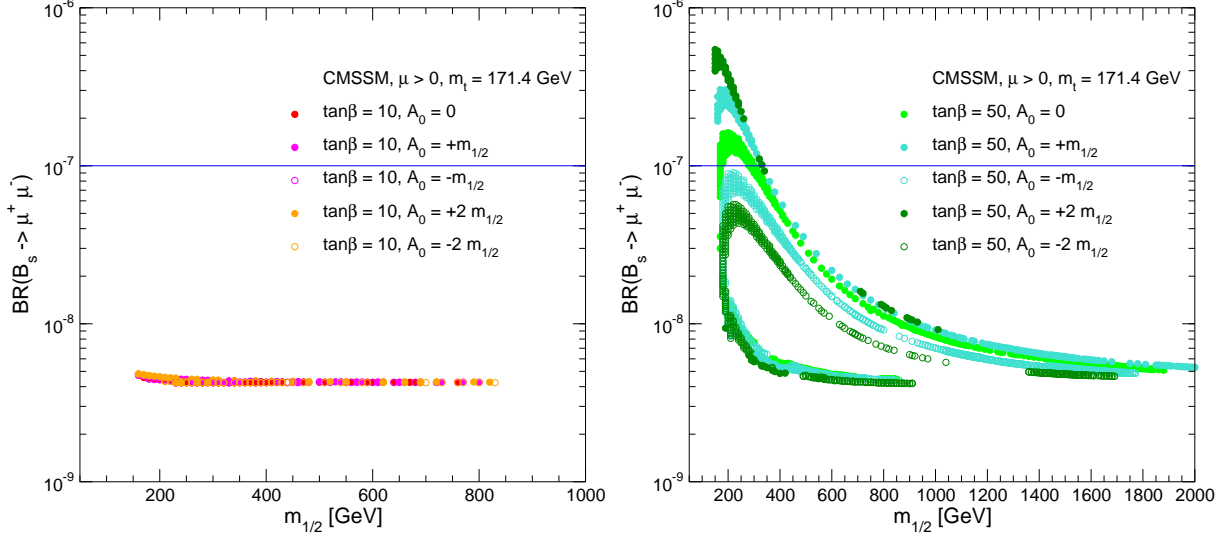


Figure 7: The CMSSM predictions for $\text{BR}(B_s \rightarrow \mu^+ \mu^-)$ as functions of $m_{1/2}$ along the WMAP strips for $\tan \beta = 10$ (left) and $\tan \beta = 50$ (right) and various choices of A_0 . The solid line indicates the current experimental 95% C.L. exclusion bound.

within scenarios with minimal flavor violation such as the CMSSM and the NUHM, the ratio of the MSSM result over the SM result can be written as

$$\frac{\text{BR}(B_u \rightarrow \tau \nu_\tau)_{\text{MSSM}}}{\text{BR}(B_u \rightarrow \tau \nu_\tau)_{\text{SM}}} = \left[1 - \left(\frac{m_{B_u}^2}{M_{H^\pm}^2} \right) \frac{\tan^2 \beta}{1 + \varepsilon_0 \tan \beta} \right]^2. \quad (34)$$

Here ε_0 denotes the effective coupling of the charged Higgs boson to up- and down-type quarks, see Ref. [102] for details. The deviation of the experimental result from the SM prediction can be expressed as

$$\frac{\text{BR}(B_u \rightarrow \tau \nu_\tau)_{\text{epx}}}{\text{BR}(B_u \rightarrow \tau \nu_\tau)_{\text{SM}}} = 0.93 \pm 0.41, \quad (35)$$

where the error includes the experimental error as well as the parametric errors from the various SM inputs. We use eq. (34) for our theory evaluation, which can then be compared with eq. (35), provided that the value of ΔM_{B_d} agrees sufficiently well in the SM and in the MSSM (which we assume here). As an error estimate we use the combined experimental and parametric error from eq. (35), an estimated intrinsic error of $\sim 2\%$, and in the CMSSM, as for $\text{BR}(B_s \rightarrow \mu^+ \mu^-)$, an additional parametric error from M_{H^\pm} , evaluated from RGE running. These errors have been added in quadrature.

We show in Fig. 8 the theoretical results for the ratio of CMSSM/SM for $\text{BR}(B_u \rightarrow \tau \nu_\tau)$ as functions of $m_{1/2}$ for $\tan \beta = 10, 50$. These results are also compared with the present

experimental result. The central (solid) line indicates the current experimental central value, and the other solid (dotted) lines show the current $\pm 1(2)$ - σ ranges from eq. (35). For $\tan\beta = 10$ the SM result is reproduced over most of the parameter space. Only very small $m_{1/2}$ values give a ratio visibly smaller than 1. For $\tan\beta = 50$ the result varies strongly between 0 and 1, and the CMSSM could easily account for the small deviation of the central value of the experimental result from the SM prediction, should that become necessary. The prediction in the focus-point region is somewhat closer to the SM value.

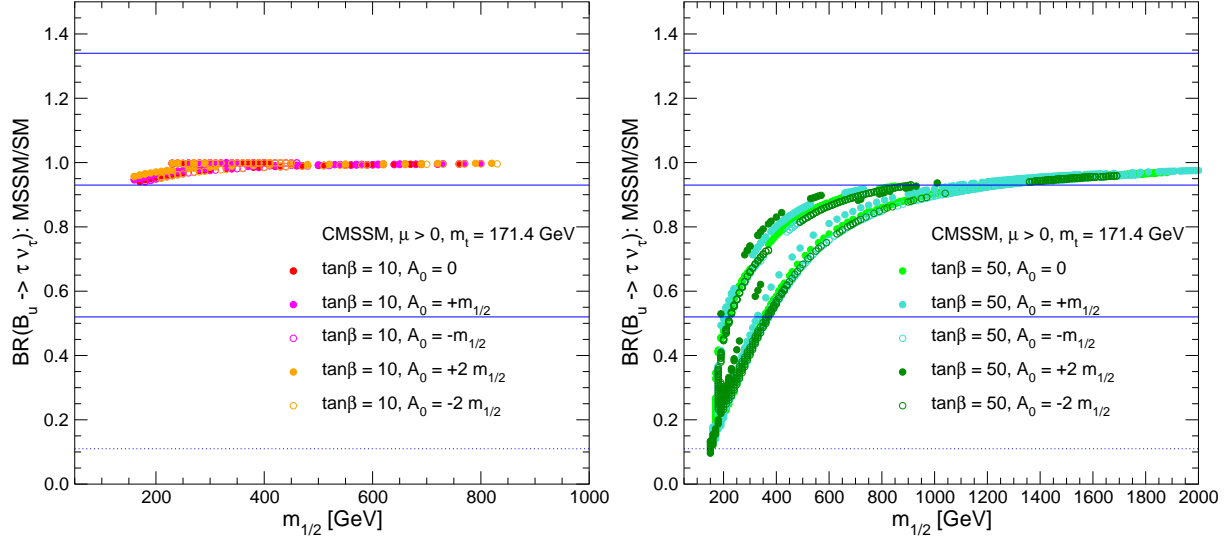


Figure 8: The predictions for the ratio CMSSM/SM for $BR(B_u \rightarrow \tau \nu_\tau)$ as functions of $m_{1/2}$ along the WMAP strips for $\tan\beta = 10$ (left) and $\tan\beta = 50$ (right) and various choices of A_0 . The central (solid) line indicates the current experimental central value, and the other solid (dotted) lines show the current $\pm 1(2)$ - σ ranges.

2.10 The $B_s-\bar{B}_s$ Mass Difference ΔM_{B_s}

The $B_s-\bar{B}_s$ oscillation frequency and consequently the $B_s-\bar{B}_s$ mass difference has recently been measured by the CDF Collaboration [103],

$$(\Delta M_{B_s})_{\text{exp}} = 17.77 \pm 0.12 \text{ ps}^{-1}, \quad (36)$$

which is compatible with the broader range of the result from D0 [104].

We follow Ref. [102] for the theory evaluation. The main MSSM contribution to the $B_s-\bar{B}_s$ oscillation comes from the exchange of neutral Higgs bosons, but we use here the full

result given in Ref. [102] (taken from Ref. [105]), where the leading dependence is given as

$$1 - \frac{(\Delta M_{B_s})_{\text{MSSM}}}{(\Delta M_{B_s})_{\text{SM}}} \sim \frac{m_b(m_b) m_s(m_b)}{M_A^2}. \quad (37)$$

The SM value, obtained from a global fit, is given by [106]

$$(\Delta M_{B_s})_{\text{SM}} = 19.0 \pm 2.4 \text{ ps}^{-1}, \quad (38)$$

resulting in

$$\frac{(\Delta M_{B_s})_{\text{exp}}}{(\Delta M_{B_s})_{\text{SM}}} = 0.93 \pm 0.13. \quad (39)$$

The error in eq. (39) is supplemented by the parametric errors in eq. (37) from $m_s(m_b) = 93 \pm 17 \text{ MeV}$ and, in the case of the CMSSM, as for $\text{BR}(B_s \rightarrow \mu^+ \mu^-)$, an additional parametric error from M_A . These errors are added in quadrature. The intrinsic error, in comparison, is assumed to be negligible.

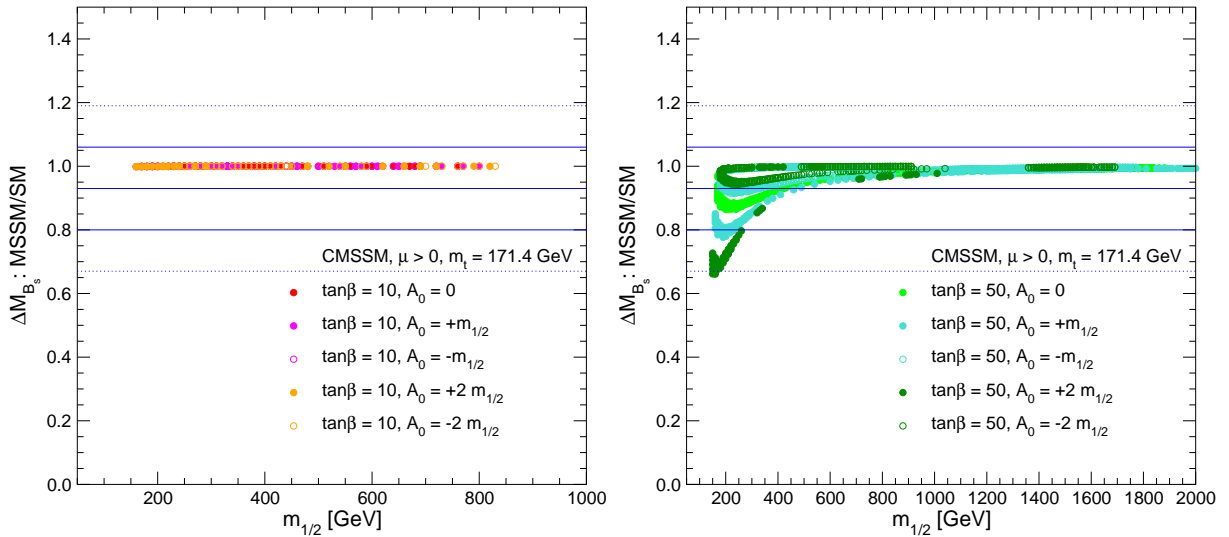


Figure 9: The predictions for the ratio CMSSM/SM for ΔM_{B_s} as functions of $m_{1/2}$ along the WMAP strips for $\tan \beta = 10$ (left) and $\tan \beta = 50$ (right) and various choices of A_0 . The central (solid) line indicates the current experimental central value, and the other solid (dotted) lines show the current $\pm 1(2)\text{-}\sigma$ ranges.

In Fig. 9 we show the results for the ratio of CMSSM/SM for ΔM_{B_s} as functions of $m_{1/2}$ for $\tan \beta = 10, 50$. These are also compared with the present experimental result. The central (solid) line indicates the current experimental central value, and the other solid (dotted) lines show the current $\pm 1(2)\text{-}\sigma$ ranges from eq. (39). For $\tan \beta = 10$ the SM result is reproduced over the whole parameter space. Only for $\tan \beta = 50$ and $m_{1/2} \lesssim 500 \text{ GeV}$ in

the coannihilation region can the CMSSM prediction be significantly lower than 1. Here the CMSSM could account for the small deviation of the experimental result from the central value SM prediction, should that be necessary.

3 CMSSM Analysis Including EWPO and BPO

We now use the analyses of the previous Section to estimate the combined χ^2 function for the CMSSM as a function of $m_{1/2}$, using the master formula (1). As a first step, Fig. 10 displays the χ^2 distribution for the EWPO alone.

In the case $\tan\beta = 10$ (left panel of Fig. 10), we see a well-defined minimum of χ^2 for $m_{1/2} \sim 300$ GeV when $A_0 > 0$, which disappears for large negative A_0 and is not present in the focus-point region. The rise at small $m_{1/2}$ is due both to the lower limit on M_h coming from the direct search at LEP and to $(g-2)_\mu$, whilst the rise at large $m_{1/2}$ is mainly due to $(g-2)_\mu$ (see Fig. 4). The measurement of M_W (see Fig. 1) leads to a slightly lower minimal value of χ^2 , but there are no substantial contributions from any of the other EWPO. The preference for $A_0 > 0$ in the coannihilation region is due to M_h (see Fig. 5), and the relative disfavour for the focus-point regions is due to its mismatch with $(g-2)_\mu$ (see Fig. 4).

In the case $\tan\beta = 50$ (right panel of Fig. 10), we again see a well-defined minimum of χ^2 , this time for $m_{1/2} \sim 400$ to 500 GeV, which is similar for all the studied values of A_0 . In this case, there is also a similar minimum of χ^2 for the focus-point region at $m_{1/2} \sim 200$ GeV. The increase in χ^2 at small $m_{1/2}$ is due to $(g-2)_\mu$ as well as M_h , whereas the increase at large $m_{1/2}$ is essentially due to $(g-2)_\mu$. We note that the overall minimum of $\chi^2 \sim 2$ is similar for both values of $\tan\beta$, and represents an excellent fit in each case.

Fig. 11 shows the corresponding combined χ^2 for the BPO alone. For both values of $\tan\beta$, these prefer large values of $m_{1/2}$, reflecting the fact that there is no hint of any deviation from the SM, and the overall quality of the fit is good. Small values of $m_{1/2}$ are disfavoured, particularly in the coannihilation region with $A_0 > 0$, mainly due to $b \rightarrow s\gamma$. The focus-point region is generally in very good agreement with the BPO data, except at very low $m_{1/2} \lesssim 400$ GeV for $\tan\beta = 50$.

Finally, we show in Fig. 12 the combined χ^2 values for the EWPO and BPO, computed in accordance with eq. (1). We see that the global minimum of $\chi^2 \sim 4.5$ for both values of $\tan\beta$. This is quite a good fit for the number of experimental observables being fitted, and the $\chi^2/\text{d.o.f.}$ is similar to the one for the EWPO alone. This increase in the total χ^2 reflects the fact that the BPO exhibit no tendency to reinforce the preference of the EWPO for small $m_{1/2}$: rather the reverse, in fact. For both values of $\tan\beta$, the focus-point region is

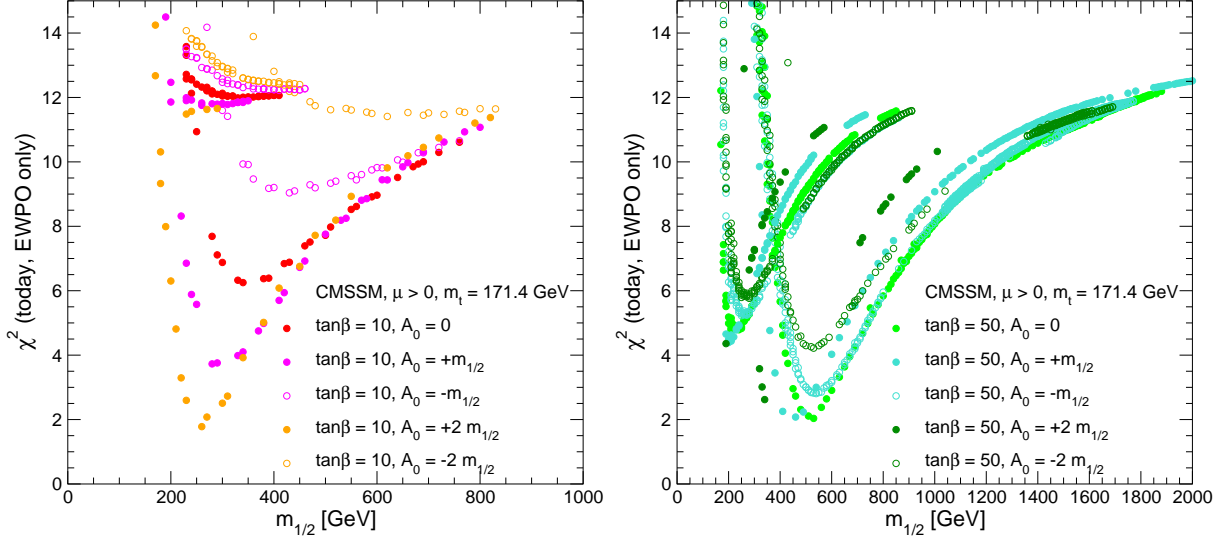


Figure 10: The combined χ^2 function for the electroweak observables M_W , $\sin^2 \theta_{\text{eff}}$, Γ_Z , $(g-2)_\mu$ and M_h , evaluated in the CMSSM for $\tan \beta = 10$ (left) and $\tan \beta = 50$ (right) for various discrete values of A_0 . We use $m_t = 171.4 \pm 2.1$ GeV and $m_b(m_b) = 4.25 \pm 0.11$ GeV, and m_0 is chosen to yield the central value of the cold dark matter density indicated by WMAP and other observations for the central values of m_t and $m_b(m_b)$.

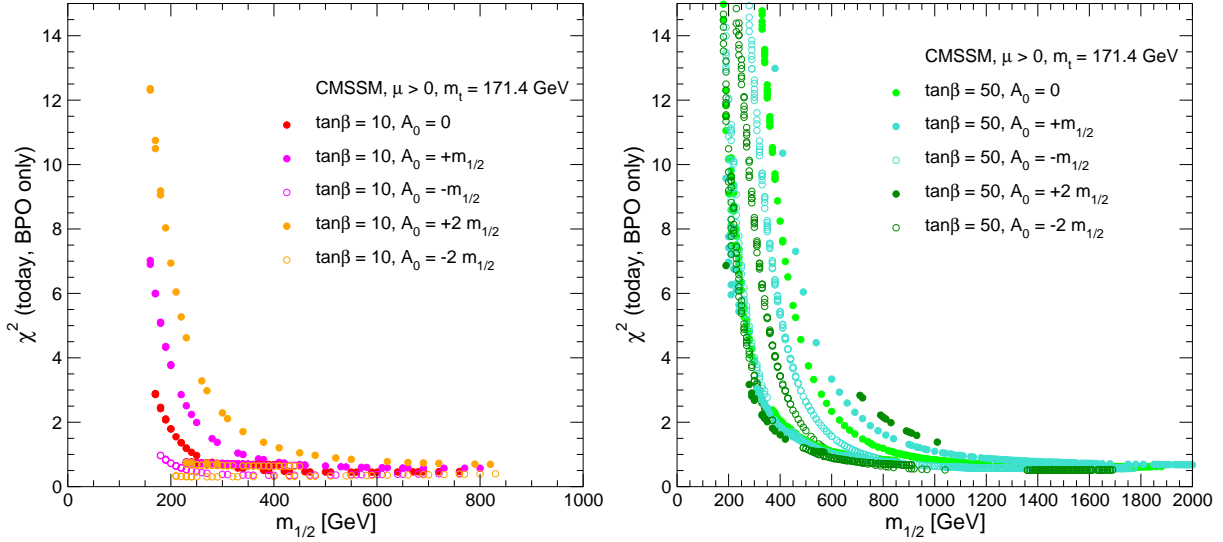


Figure 11: The combined χ^2 function for the b physics observables $\text{BR}(b \rightarrow s\gamma)$, $\text{BR}(B_s \rightarrow \mu^+\mu^-)$, $\text{BR}(B_u \rightarrow \tau\nu_\tau)$ and ΔM_{B_s} , evaluated in the CMSSM for $\tan \beta = 10$ (left) and $\tan \beta = 50$ (right) for various discrete values of A_0 . We use $m_t = 171.4 \pm 2.1$ GeV and $m_b(m_b) = 4.25 \pm 0.11$ GeV, and m_0 is chosen to yield the central value of the cold dark matter density indicated by WMAP and other observations for the central values of m_t and $m_b(m_b)$.

disfavoured by comparison with the coannihilation region, though this effect is less important for $\tan\beta = 50$. For $\tan\beta = 10$, $m_{1/2} \sim 300$ GeV and $A_0 > 0$ are preferred, whereas, for $\tan\beta = 50$, $m_{1/2} \sim 600$ GeV and $A_0 < 0$ are preferred. This change-over is largely due to the impact of the LEP M_h constraint for $\tan\beta = 10$ and the $b \rightarrow s\gamma$ constraint for $\tan\beta = 50$.

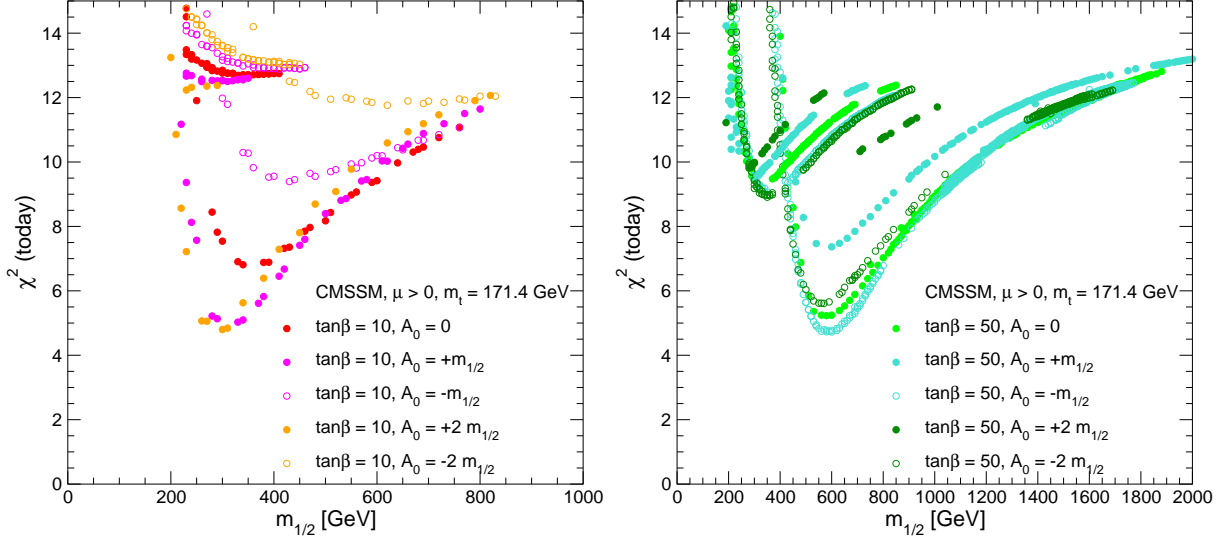


Figure 12: The combined χ^2 function for the electroweak observables M_W , $\sin^2\theta_{\text{eff}}$, Γ_Z , $(g-2)_\mu$, M_h , and the b physics observables $\text{BR}(b \rightarrow s\gamma)$, $\text{BR}(B_s \rightarrow \mu^+\mu^-)$, $\text{BR}(B_u \rightarrow \tau\nu_\tau)$ and ΔM_{B_s} , evaluated in the CMSSM for $\tan\beta = 10$ (left) and $\tan\beta = 50$ (right) for various discrete values of A_0 . We use $m_t = 171.4 \pm 2.1$ GeV and $m_b(m_b) = 4.25 \pm 0.11$ GeV, and m_0 is chosen to yield the central value of the cold dark matter density indicated by WMAP and other observations for the central values of m_t and $m_b(m_b)$.

We display in Fig. 13 the χ^2 functions for various SUSY masses in the CMSSM for $\tan\beta = 10$, including (a) $m_{\tilde{\chi}_1^0}$, (b) $m_{\tilde{\chi}_2^0}$ and $m_{\tilde{\chi}_1^\pm}$ (which are very similar), (c) $m_{\tilde{\tau}_1}$, (d) M_A , (e) $m_{\tilde{t}_1}$ and (f) $m_{\tilde{g}}$. We see two distinct populations of points, corresponding to the $\chi - \tilde{\tau}_1$ coannihilation (which is favoured) and focus-point regions (which is disfavoured). In the latter region, very low values of $m_{1/2}$ are preferred, as can be seen in panels (a) and (f), relatively small values of μ , as can be seen in panel (b), large values of m_0 , as can be seen in panels (c) and (e), and large values of M_A , as can (not) be seen in panel (d). Compared to the analysis in Ref. [9], where $\text{BR}(b \rightarrow s\gamma)$ was the only BPO included, and where a top quark mass of 172.7 GeV was used, there is no significant shift of the values of the masses where χ^2 has its minimum, which is in the coannihilation region. As before, the present analysis gives hope for seeing squarks and gluinos in the early days of the LHC (panels (e) and (f)), and also hope for seeing charginos, neutralinos and staus at the ILC (panels (a), (b) and (c)), whereas observing the heavier Higgs bosons would be more challenging (panel (d)).

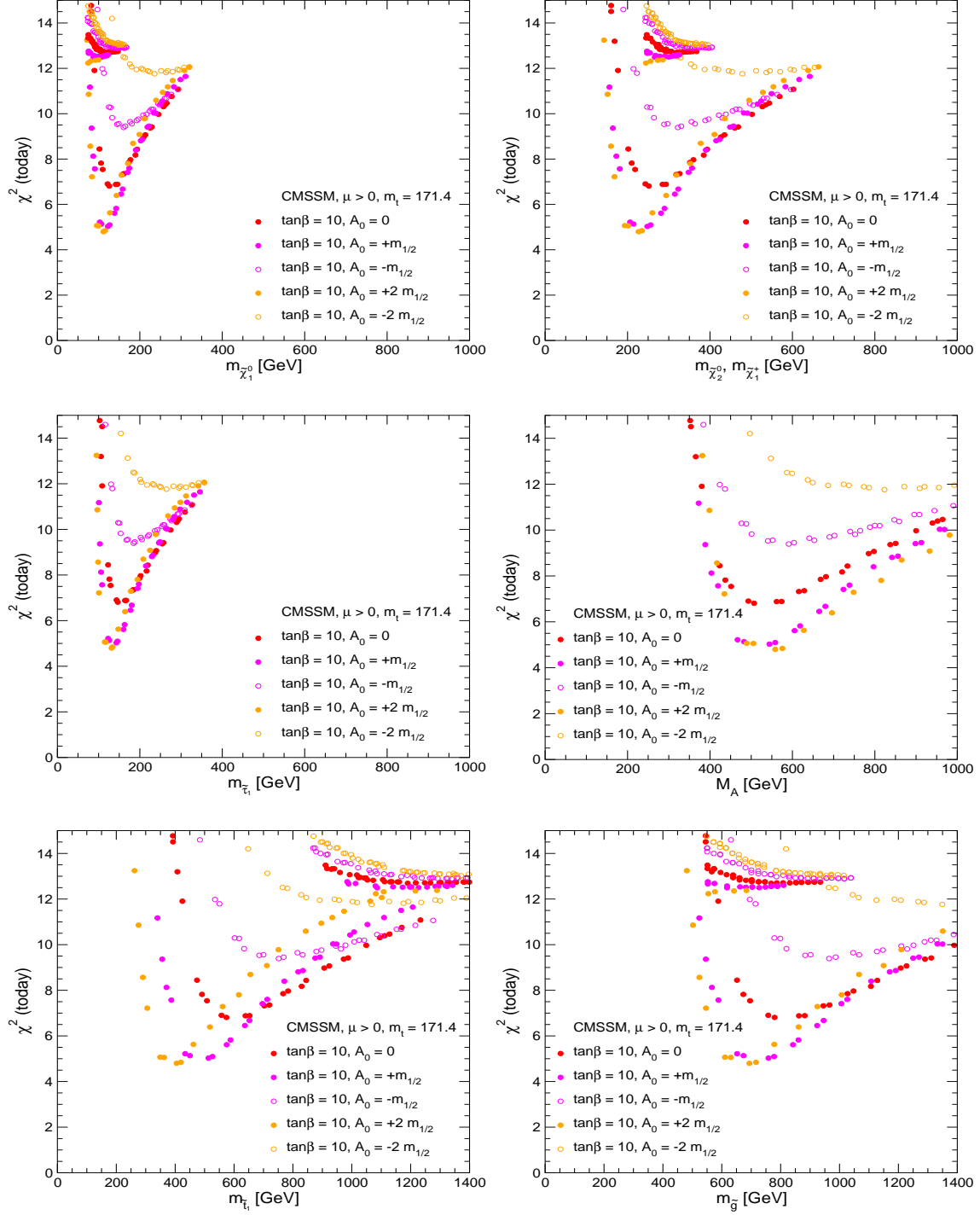


Figure 13: Various SUSY masses are presented with their respective χ^2 value in the CMSSM for $\tan\beta = 10$. The panels show (a) $m_{\tilde{\chi}_1^0}$, (b) $m_{\tilde{\chi}_2^0}$ and $m_{\tilde{\chi}_1^\pm}$ (which are very similar), (c) $m_{\tilde{\tau}_1}$, (d) M_A , (e) $m_{\tilde{t}_1}$ and (f) $m_{\tilde{g}}$.

In Fig. 14 we show the analogous χ^2 functions for various SUSY masses in the CMSSM for $\tan\beta = 50$: (a) $m_{\tilde{\chi}_1^0}$, (b) $m_{\tilde{\chi}_2^0}$ and $m_{\tilde{\chi}_1^\pm}$ (which are very similar), (c) $m_{\tilde{\tau}_1}$, (d) M_A , (e) $m_{\tilde{t}_1}$ and (f) $m_{\tilde{g}}$. We again see the clear separation between the focus-point and coannihilation regions, interpolated by a light-Higgs pole strip, and that the coannihilation region is somewhat preferred. As for lower $\tan\beta$, small values of $m_{1/2}$ and larger values of m_0 are preferred, and also small values of μ and larger values of M_A . Again as for $\tan\beta = 10$, compared to the analysis in Ref. [9], where $\text{BR}(b \rightarrow s\gamma)$ was the only BPO included and where a top quark mass of 172.7 GeV was used, we do not find a significant shift in the values of the masses with lowest χ^2 . The sparticle masses are generally higher than for $\tan\beta = 10$: finding squarks and gluinos should still be ‘easy’ at the LHC, but seeing charginos, neutralinos and staus at the ILC would be more challenging, depending on its center-of-mass energy.

Analogously to the sparticle masses in Figs. 13 and 14, we display in Fig. 15 the total χ^2 functions for M_h , as calculated in the CMSSM for $\tan\beta = 10$ (left panel) and $\tan\beta = 50$ (right panel). We recall that this theoretical prediction has an intrinsic uncertainty of $\sim \pm 1.5$ GeV, which should be combined with the experimental error in m_t . It is a clear prediction of this analysis that M_h should be very close to the LEP lower limit, and probably $\lesssim 120$ GeV, though a value as large as ~ 123 GeV is possible (but is χ^2 disfavoured), particularly if $\tan\beta = 50$.

In the case of the SM, it is well known that tension between the lower limit on M_h from the LEP direct search and the relatively low value of M_h preferred by the EWPO has recently been increasing [30, 31]. This tension is strongly reduced within the CMSSM, particularly for $\tan\beta = 50$. We display in Fig. 16 the global χ^2 functions for the EWPO and BPO, but this time *omitting* the contribution for the LEP Higgs search. This corresponds to the fitted value of M_h in the CMSSM. Comparing Fig. 16 and Fig. 15, we see that all data (excluding M_h) favour a value of $M_h \sim 110$ GeV if $\tan\beta = 10$ and $M_h \sim 115$ GeV if $\tan\beta = 50$. On the other hand, the currently best-fit value of M_H^{SM} is 76 GeV [30], i.e. substantially below the SM LEP bound of 114.4 GeV [78]. In comparison to the favoured values *including* the LEP limits we get a ~ 5 GeV smaller value of M_h if $\tan\beta = 10$, whereas the difference is only ~ 1 GeV if $\tan\beta = 50$.⁹ Correspondingly, comparing Fig. 16 and Fig. 15, we see that the LEP limit increases the value of χ^2 by ~ 3.5 for the $\tan\beta = 10$ case, but by only ~ 1 for the $\tan\beta = 50$ case. However, we emphasize that for both cases there are quite good global fits to all the EWPO and BPO with $\chi^2 \sim 4.5$.

⁹We also recall that the estimated theoretical uncertainty in M_h for fixed values of the CMSSM parameters is ± 3 GeV.

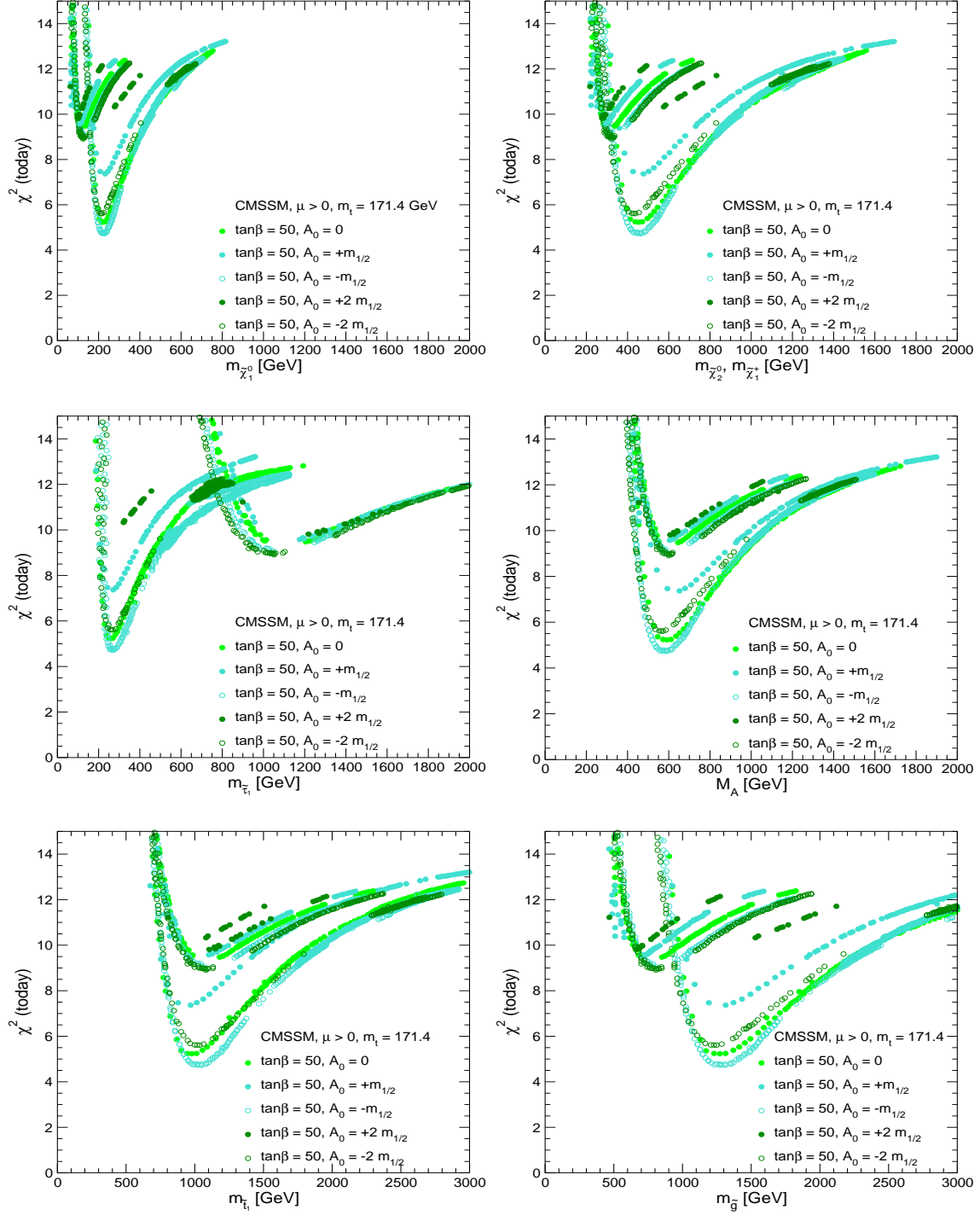


Figure 14: Various SUSY masses are presented with their respective χ^2 value in the CMSSM for $\tan\beta = 50$. The panels show (a) $m_{\tilde{\chi}_1^0}$, (b) $m_{\tilde{\chi}_2^0}$ and $m_{\tilde{\chi}_1^\pm}$ (which are very similar), (c) $m_{\tilde{\tau}_1}$, (d) M_A , (e) $m_{\tilde{t}_1}$ and (f) $m_{\tilde{g}}$.

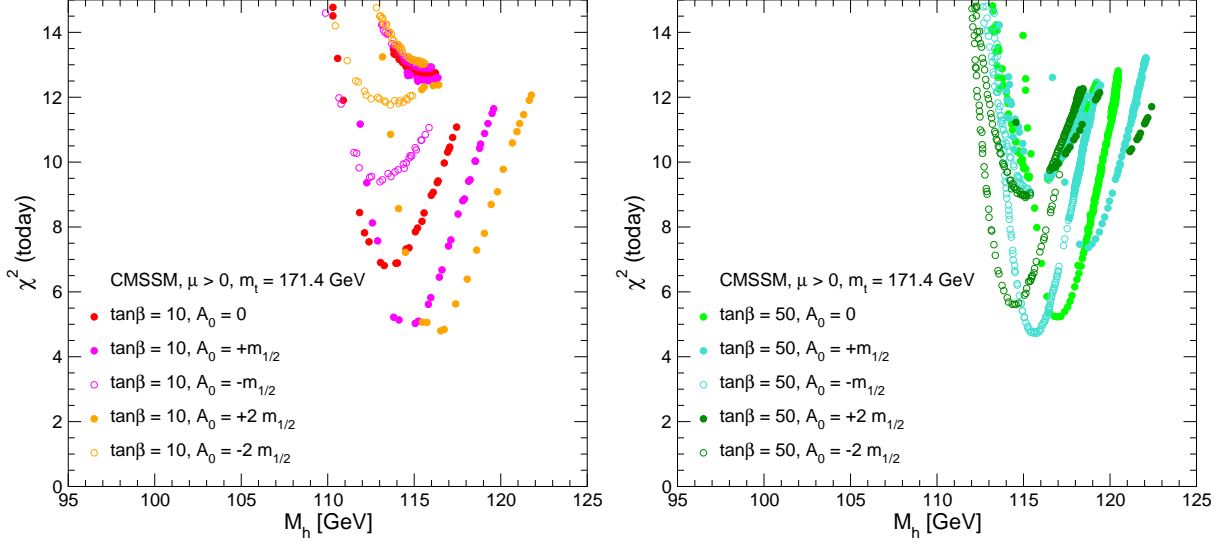


Figure 15: The combined χ^2 function for M_h , as obtained from the combined analysis of all EWPO and BPO, evaluated in the CMSSM for $\tan\beta = 10$ (left) and $\tan\beta = 50$ (right) for various discrete values of A_0 . We use $m_t = 171.4 \pm 2.1$ GeV and $m_b(m_b) = 4.25 \pm 0.11$ GeV, and m_0 is chosen to yield the central value of the cold dark matter density indicated by WMAP and other observations for the central values of m_t and $m_b(m_b)$.

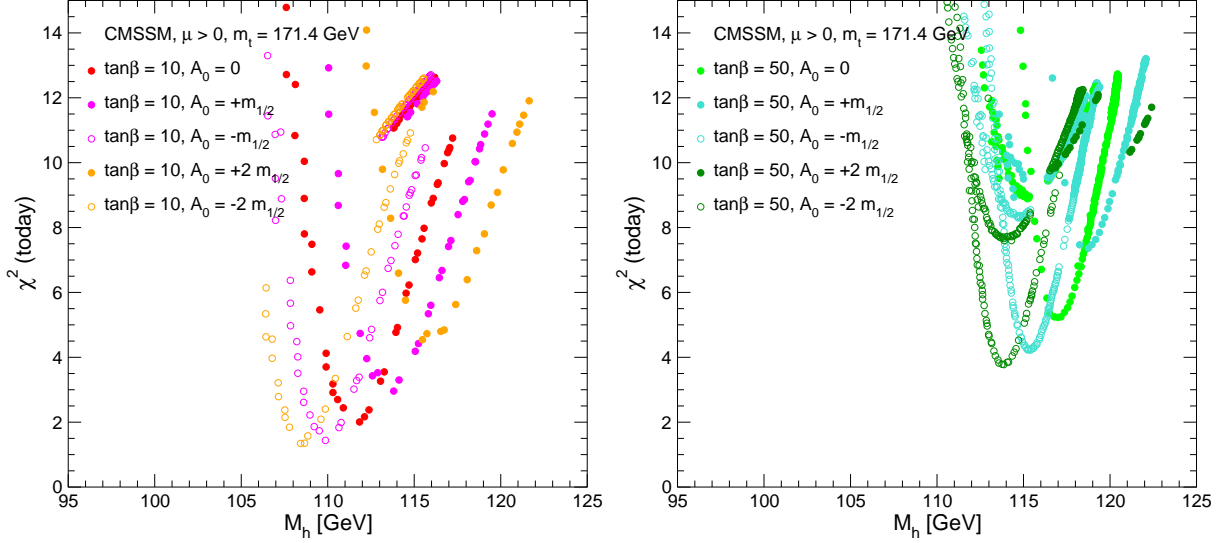


Figure 16: The combined χ^2 function for M_h , as obtained from a combined analysis of all EWPO and BPO *except* the LEP Higgs search, as evaluated in the CMSSM for $\tan\beta = 10$ (left) and $\tan\beta = 50$ (right) for various discrete values of A_0 . We use $m_t = 171.4 \pm 2.1$ GeV and $m_b(m_b) = 4.25 \pm 0.11$ GeV, and m_0 is chosen to yield the central value of the cold dark matter density indicated by WMAP and other observations for the central values of m_t and $m_b(m_b)$.

4 NUHM Analysis Including EWPO and BPO

The CMSSM is a very particular case of the general MSSM. It has a manageable parameter space, but may not be able to capture all the possibilities available in the general MSSM. Specifically, as we have seen, while providing a better fit to the EWPO than the SM, it provides no improvement for the BPO, and there is a slight tension between the EWPO and the BPO within the restrictive CMSSM framework. For these and other reasons, we now consider the NUHM. The dimensionality of the MSSM parameter space is increased by a manageable amount compared to the CMSSM, namely two extra dimensions. Moreover, there was no strong phenomenological motivation for assuming universality for the Higgs masses, and there is reason to hope that relaxing the Higgs universality assumption may help reconcile the EWPO and BPO. As we have seen, the EWPO prefer a specific range of $m_{1/2}$ (~ 300 GeV for $\tan\beta = 10$ and ~ 500 GeV for $\tan\beta = 50$) in the coannihilation region, and disfavour the focus-point region (particularly for $\tan\beta = 10$). Within the CMSSM, the electroweak vacuum conditions fix the corresponding values of $|\mu|$ and M_A . These values are not very crucial for the EWPO, but are potentially important for the BPO. For example, the extra MSSM contribution to $b \rightarrow s\gamma$ is small only if the supplementary charged-Higgs and chargino diagrams cancel to some extent, which imposes a specific condition on their masses. This may not be satisfied within the CMSSM, but is not incompatible *a priori* with the NUHM, in which $|\mu|$ and M_A become (to some extent) free parameters.

Just as we focused attention in the previous CMSSM analysis on WMAP lines in parameter space, where the cold dark matter density falls within the range allowed by WMAP and other astrophysical and cosmological observations, we also focus on ‘WMAP surfaces’ in the NUHM parameter space. Many NUHM parameter planes have been considered in the past [5, 6, 107] and, as in the CMSSM, generically the dark matter constraint is satisfied only in thin strips in each NUHM plane. Many phenomenological studies of MSSM Higgs physics have analyzed the possibilities in $(M_A, \tan\beta)$ planes under different hypotheses for other MSSM parameters. In particular, in the general MSSM framework, $(M_A, \tan\beta)$ planes have been suggested for phenomenological Higgs physics analyses [108–110], neglecting the constraints coming from CDM. In the NUHM, in order to keep the dark matter density within the WMAP range across generic regions of such a $(M_A, \tan\beta)$ plane, one must adjust one or more of the free parameters continuously across the plane. We propose here two strategies for specifying suitable parameter scans.

We consider first a typical $(M_A, \tan\beta)$ plane for fixed $m_0, m_{1/2}$ and μ , as shown for example in Fig. 5a of Ref. [5], where the choices $m_0 = 800$ GeV, $m_{1/2} = 600$ GeV and

$\mu = 1000$ GeV were made. In this example, the relic density exceeds the WMAP upper limit almost everywhere in the $(M_A, \tan\beta)$ plane, except along a narrow vertical strip where $m_{\tilde{\chi}_1^0} \sim M_A/2$, and rapid direct-channel annihilation suppresses the relic density below the WMAP range. On either side of this strip, there are thin regions where the relationship between M_A and $m_{1/2}$ is such that the relic density falls within the WMAP range whatever the value of $\tan\beta$. Building on this observation, we study a $(M_A, \tan\beta)$ plane **P1** with the same values of $m_0 = 800$ GeV and $\mu = 1000$ GeV, but with $m_{1/2}$ chosen to vary across the plane so as to maintain the WMAP relationship with M_A :

$$\frac{9}{8}M_A - 12.5 \text{ GeV} \leq m_{1/2} \leq \frac{9}{8}M_A + 37.5 \text{ GeV}. \quad (40)$$

As we saw earlier, within the CMSSM, smaller values of m_0 are preferred. We therefore consider also a $(M_A, \tan\beta)$ plane **P2** with the fixed values $m_0 = 300$ GeV and $\mu = 800$ GeV, and $m_{1/2}$ again adjusted continuously across the plane so as to maintain the WMAP relationship with M_A :

$$1.2M_A - 40 \text{ GeV} \leq m_{1/2} \leq 1.2M_A + 40 \text{ GeV}. \quad (41)$$

Many more examples could be chosen, but these serve as representative examples of NUHM planes that enable us to explore the possibility of reducing the tension between the EWPO and BPO.

We also consider two more examples, inspired by the (μ, M_A) planes also shown in Ref. [5]. There we see that, for fixed values of $m_{1/2}$ and m_0 , there is a ‘magic’ value of $\mu > 0$ which provides a suitable value of the relic density for almost all values of M_A , the exception being a narrow strip around the rapid-annihilation funnel where $m_{\tilde{\chi}_1^0} \sim M_A/2$. The value of μ varies with $\tan\beta$, but a suitable scan yields a $(M_A, \tan\beta)$ plane where the relic density falls within the WMAP range for all except a sliver of M_A values that broadens somewhat as $\tan\beta$ increases. Within this sliver, the relic density falls below the WMAP range: this region is therefore not incompatible with cosmology, but would require a supplementary source of cold dark matter. One example of such a plane, **P3**, has fixed $m_{1/2} = 500$ GeV and $m_0 = 1000$ GeV, with μ in the range

$$\mu = 250 - 400 \text{ GeV}. \quad (42)$$

The other example **P4** has fixed $m_{1/2} = 300$ GeV and $m_0 = 300$ GeV, with μ in the range

$$\mu = 200 - 350 \text{ GeV}. \quad (43)$$

The four scenarios are summarized in Tab. 1. In the analyses below, we quote the minimal values of χ^2 for values of μ within the ranges (42), (43), for the planes **P3** and **P4**, respectively.

	$m_{1/2}$	m_0	A_0	μ
P1	varied	800	0	1000
P2	varied	300	0	800
P3	500	1000	0	varied
P4	300	300	0	varied

Table 1: The four NUHM scenarios, with M_A and $\tan\beta$ kept as free parameters. All masses are in GeV.

We now consider the most important contributions to the likelihood functions for these four $(M_A, \tan\beta)$ planes.

The principal contributions to the overall χ^2 value, and hence also to the likelihood function, for the $(M_A, \tan\beta)$ plane for scenario **P1** are shown in Fig. 17. We see in panel (a) that the χ^2 value of a_μ is not very satisfactory anywhere in the plane, but particularly not at large M_A and small $\tan\beta$. Panel (b) shows that the LEP lower limit on M_h disfavours $M_A < 300$ GeV in this scenario. Small values of M_A are also disfavoured by $b \rightarrow s\gamma$, as seen in panel (c), and large values of M_A and $\tan\beta$ are also disfavoured, but to a lesser extent. Panels (d) and (e) show that large values of $\tan\beta$ and small values of M_A are disfavoured by both $B_s \rightarrow \mu^+\mu^-$ and $B_u \rightarrow \tau\nu_\tau$. Finally, panel (f) shows the values of the combined EWPO and BPO χ^2 function for scenario **P1** throughout the $(M_A, \tan\beta)$ plane. We see that the best-fit point has $M_A \sim 440$ GeV and $\tan\beta \sim 50$. This is the optimal compromise between a_μ and $b \rightarrow s\gamma$ that also respects the M_h and other BPO constraints. We note that this best-fit point has $\chi^2 = 7.1$, which is not a significant improvement, but even slightly worse than the CMSSM fits discussed in the previous Section. We also display in panel (f) of Fig. 17 the $\Delta\chi^2 = 2.30$ and 4.61 contours, which would correspond to the 68 % and 95 % C.L. contours in the $(M_A, \tan\beta)$ plane *if* the overall likelihood distribution, $\mathcal{L} \propto e^{-\chi^2/2}$, was Gaussian. This is clearly only roughly the case in this analysis, but these contours nevertheless give interesting indications on the preferred region in the $(M_A, \tan\beta)$ plane.

We do not show results in the upper right corners of these planes (with high M_A and high $\tan\beta$) because there the relic density in this region is low compared to the preferred WMAP value. In this region, for the choice of m_0 and μ and the range of $m_{1/2}$ given in eq. (40), we are sitting too close to the funnel. However, these points could be brought into agreement with WMAP, by extending the sampled range in $m_{1/2}$ to lower values. The lower left portions of these planes are missing because of the finite resolution of our scan. In these

regions of fixed low values of M_A and $\tan\beta$, the relic density is very sensitive to $m_{1/2}$, and viable points are missed with the resolution in $m_{1/2}$ of 10 GeV that we use. One final remark on Fig. 17 concerns high values of $\tan\beta$. At values of $\tan\beta > 52$, the RGE evolution may break down due to a tendency towards a divergent bottom Yukawa coupling.

The principal contributions to the total χ^2 function for the $(M_A, \tan\beta)$ plane for scenario **P2** are shown in Fig. 18. We see in panel (a) that the value of a_μ is very satisfactory in a band running across the plane from $(M_A, \tan\beta) \sim (100 \text{ GeV}, 15)$ to $\sim (400 \text{ GeV}, 50)$. In particular, large values of M_A and small $\tan\beta$ are disfavoured. Panel (b) shows that the LEP lower limit on M_h disfavours $M_A < 300 \text{ GeV}$ also in this scenario. Small values of M_A are also disfavoured by $b \rightarrow s\gamma$, as seen in panel (c), and large values of M_A and $\tan\beta$ are also disfavoured, but to a lesser extent. Panels (d) and (e) show that large values of $\tan\beta$ and small values of M_A are again disfavoured by both $B_s \rightarrow \mu^+\mu^-$ and $B_u \rightarrow \tau\nu_\tau$. Finally, panel (f) shows the combined EWPO and BPO χ^2 function for scenario **P2** throughout the $(M_A, \tan\beta)$ plane. We see that the best-fit point has $M_A \sim 340 \text{ GeV}$ and $\tan\beta \sim 35$. This is a good fit to both a_μ and $b \rightarrow s\gamma$, as well as the M_h and other BPO constraints. We note that this best-fit point has $\chi^2 = 3.5$, which is a noticeable improvement on the CMSSM fits discussed in the previous Section. We note that the $\Delta\chi^2 = 2.30$ and 4.61 contours are somewhat more compact than in the case of scenario **P1**.

For the parameter choice of **P2** large values of M_A are excluded because the right-handed stau becomes the LSP. This could be avoided by lowering the value of $m_{1/2}$ outside the range in eq. (41), so as to recover a neutralino LSP. However, unless we drop $m_{1/2}$ substantially below our adopted range, the relic density will be too small due to LSP-stau coannihilations. Finally, we note that the hole around $(M_A, \tan\beta) \sim (600 \text{ GeV}, 17)$ is due to the funnel. In this hole, the relic density is far too small to supply the preferred amount of cold dark matter. However, the hole could be filled if a larger range were chosen for $m_{1/2}$.

The principal contributions to the total χ^2 function for the $(M_A, \tan\beta)$ plane for scenario **P3** are shown in Fig. 19¹⁰. We see in panel (a) that the value of a_μ is satisfactory only for very large values of $\tan\beta$, almost independently of M_A . In particular, values of $\tan\beta < 25$ are quite strongly disfavoured. Panel (b) shows that the LEP lower limit on M_h disfavours very low values of $\tan\beta$ and $M_A < 150 \text{ GeV}$ for $\tan\beta < 25$. Small values of M_A and $\tan\beta$ are also disfavoured by $b \rightarrow s\gamma$, as seen in panel (c), as also are large values of M_A and $\tan\beta$. Panels (d) and (e) show that large values of $\tan\beta$ and small values of M_A are again

¹⁰We do not display the χ^2 values in the underdense slivers of the plane.

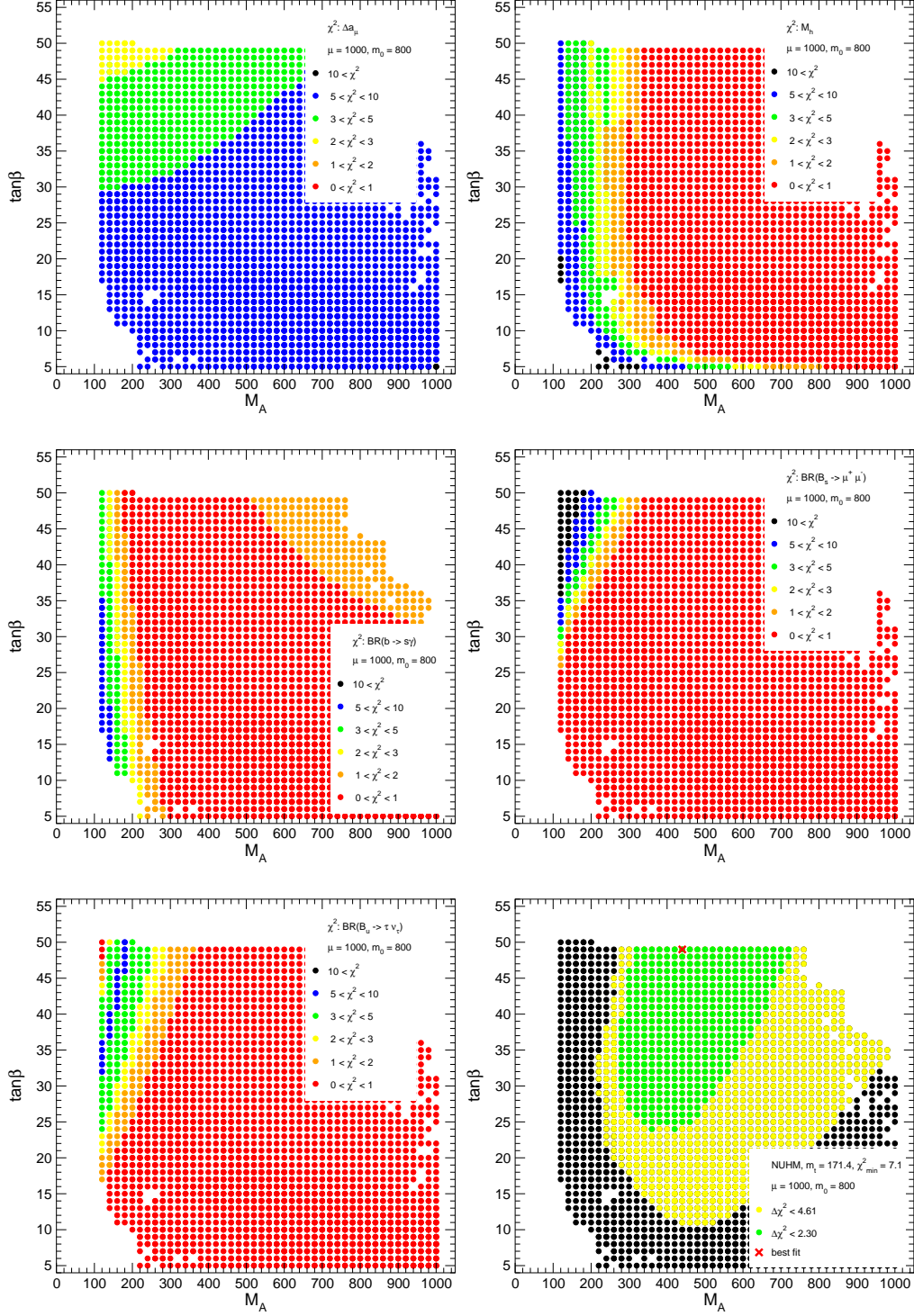


Figure 17: The most important contributions to the total χ^2 value for the NUHM ($M_A, \tan \beta$) plane **P1**, due to (a) a_μ , (b) M_h , (c) $b \rightarrow s\gamma$, (d) $B_s \rightarrow \mu^+\mu^-$ and (e) $B_u \rightarrow \tau\nu_\tau$, and (f) the combined EWPO and BPO χ^2 function. We use $m_t = 171.4 \pm 2.1$ GeV and $m_b(m_b) = 4.25 \pm 0.11$ GeV, and $m_{1/2}$ is adjusted continuously so as to yield the central value of the cold dark matter density indicated by WMAP and other observations for the central values of m_t and $m_b(m_b)$.

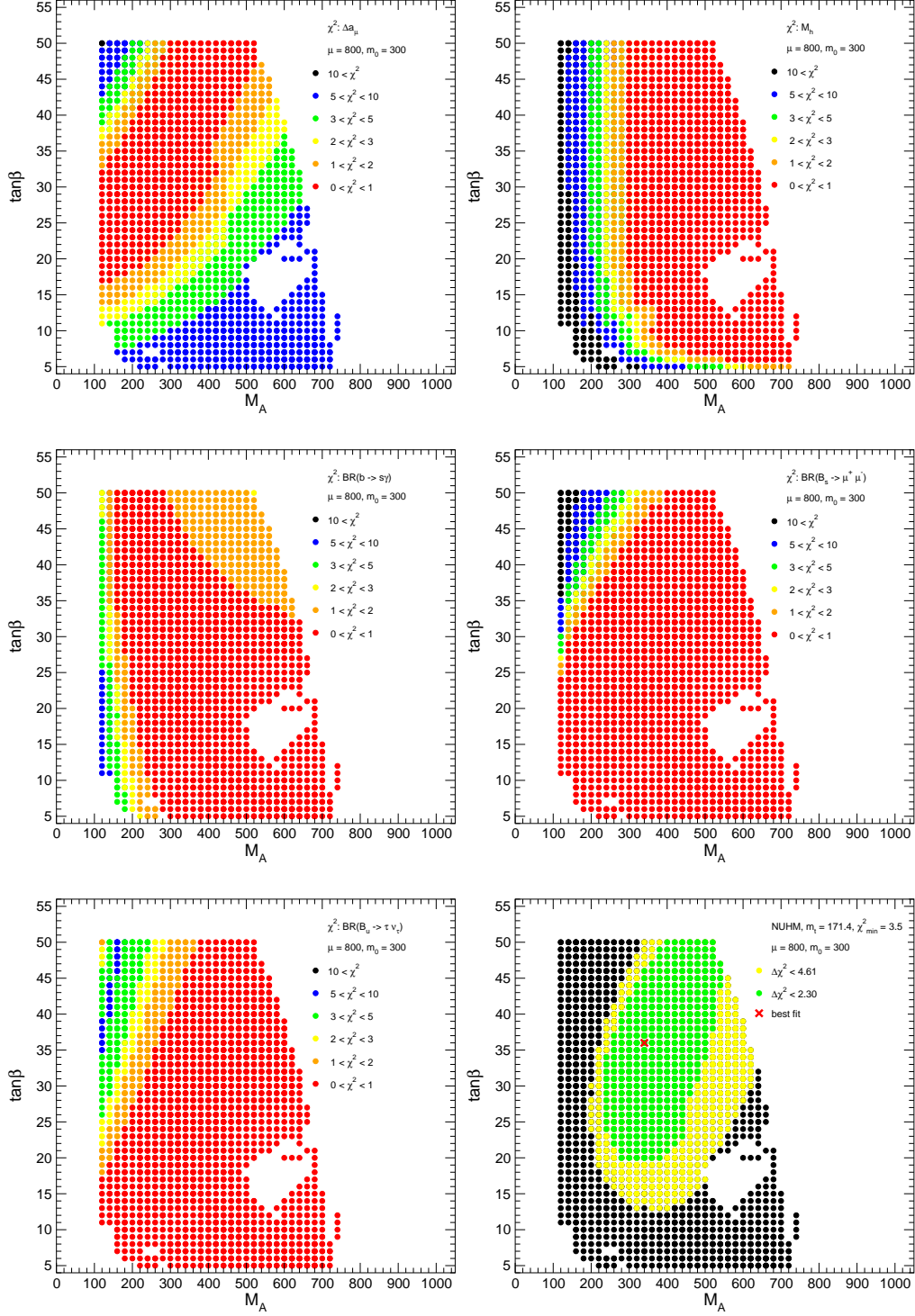


Figure 18: The most important contributions to the total χ^2 value for the NUHM ($M_A, \tan \beta$) plane **P2**, due to (a) a_μ , (b) M_h , (c) $b \rightarrow s\gamma$, (d) $B_s \rightarrow \mu^+\mu^-$ and (e) $B_u \rightarrow \tau\nu_\tau$, and (f) the combined EWPO and BPO χ^2 function. We use $m_t = 171.4 \pm 2.1$ GeV and $m_b(m_b) = 4.25 \pm 0.11$ GeV, and $m_{1/2}$ is adjusted continuously so as to yield the central value of the cold dark matter density indicated by WMAP and other observations for the central values of m_t and $m_b(m_b)$.

disfavoured by both $B_s \rightarrow \mu^+\mu^-$ and $B_u \rightarrow \tau\nu_\tau$ ¹¹. We note that ΔM_{B_s} (not shown) also disfavours small M_A and large $\tan\beta$. Finally, panel (f) shows the combined EWPO and BPO χ^2 function for scenario **P3** throughout the $(M_A, \tan\beta)$ plane. We see that the best-fit point has $M_A \sim 300$ GeV and $\tan\beta \sim 35$. This is not a very good fit to a_μ , but it is a good fit to $b \rightarrow s\gamma$, M_h and the other BPO constraints. We note that this best-fit point has $\chi^2 = 7.4$, which is *not* an improvement on the CMSSM fits discussed in the previous Section. The $\Delta\chi^2 = 2.30$ and 4.61 contours are somewhat looser than in the two previous scenarios, and extend to very large M_A .

The principal contributions to the total χ^2 function for the $(M_A, \tan\beta)$ plane for scenario **P4** are shown in Fig. 20¹². We see in panel (a) that a_μ favours a swathe with $\tan\beta \sim 15$ to 20, almost independently of M_A . In particular, values of $\tan\beta > 25$ and $\tan\beta < 5$ are quite strongly disfavoured. Panel (b) shows that the LEP lower limit on M_h disfavours values $\tan\beta < 15$, the constraint becoming stronger for $M_A < 200$ GeV. A small band of values of M_A and $\tan\beta$ are favoured by $b \rightarrow s\gamma$, as seen in panel (c), extending to $\tan\beta > 15$ only for M_A below the funnel at ~ 250 GeV. Panels (d) and (e) show the familiar feature that large values of $\tan\beta$ and small values of M_A are disfavoured by both $B_s \rightarrow \mu^+\mu^-$ and $B_u \rightarrow \tau\nu_\tau$, and the same is true for ΔM_{B_s} (not shown). Finally, panel (f) shows the combined EWPO and BPO χ^2 function for scenario **P4** throughout the $(M_A, \tan\beta)$ plane. We see that the best-fit point has $M_A \sim 200$ GeV and $\tan\beta \sim 20$. This is not a very good fit to M_h , but it is a good fit to a_μ , $b \rightarrow s\gamma$, and the other BPO constraints. We note that this best-fit point has $\chi^2 = 5.6$, which is *similar* to the CMSSM fits discussed in the previous Section. We note also that the $\Delta\chi^2 = 2.30$ and 4.61 contours are particularly tight in this scenario, and rule out very large values of M_A and/or $\tan\beta$.

There are some common features of these analyses for fixed $(m_{1/2}, m_0)$ and (m_0, μ) . For example, we find that relatively low values of $M_A \sim 200$ to 400 GeV are consistently favoured. This is essentially because a_μ prefers moderately small values of $m_{1/2}$ which would, if left to themselves, create problems for $b \rightarrow s\gamma$. However, this tension may be mitigated if M_A is correspondingly small, providing a cancellation in the supersymmetric contributions to the $b \rightarrow s\gamma$ decay amplitude. We also note a consistent preference for relatively large values of $\tan\beta \sim 20$ to 50, which is essentially due to the pressure exerted by the LEP lower limit on the Higgs mass.

As discussed above, the LSP would constitute (most of) the cold dark matter across

¹¹We note in panel (e) the appearance of a second, narrow favoured strip of parameter space. In this strip, the charged-Higgs contribution to the decay amplitude is not a small perturbation, but is $\sim -2\times$ the W^\pm contribution!

¹²Again, we do not display the χ^2 values in the underdense slivers of the plane.

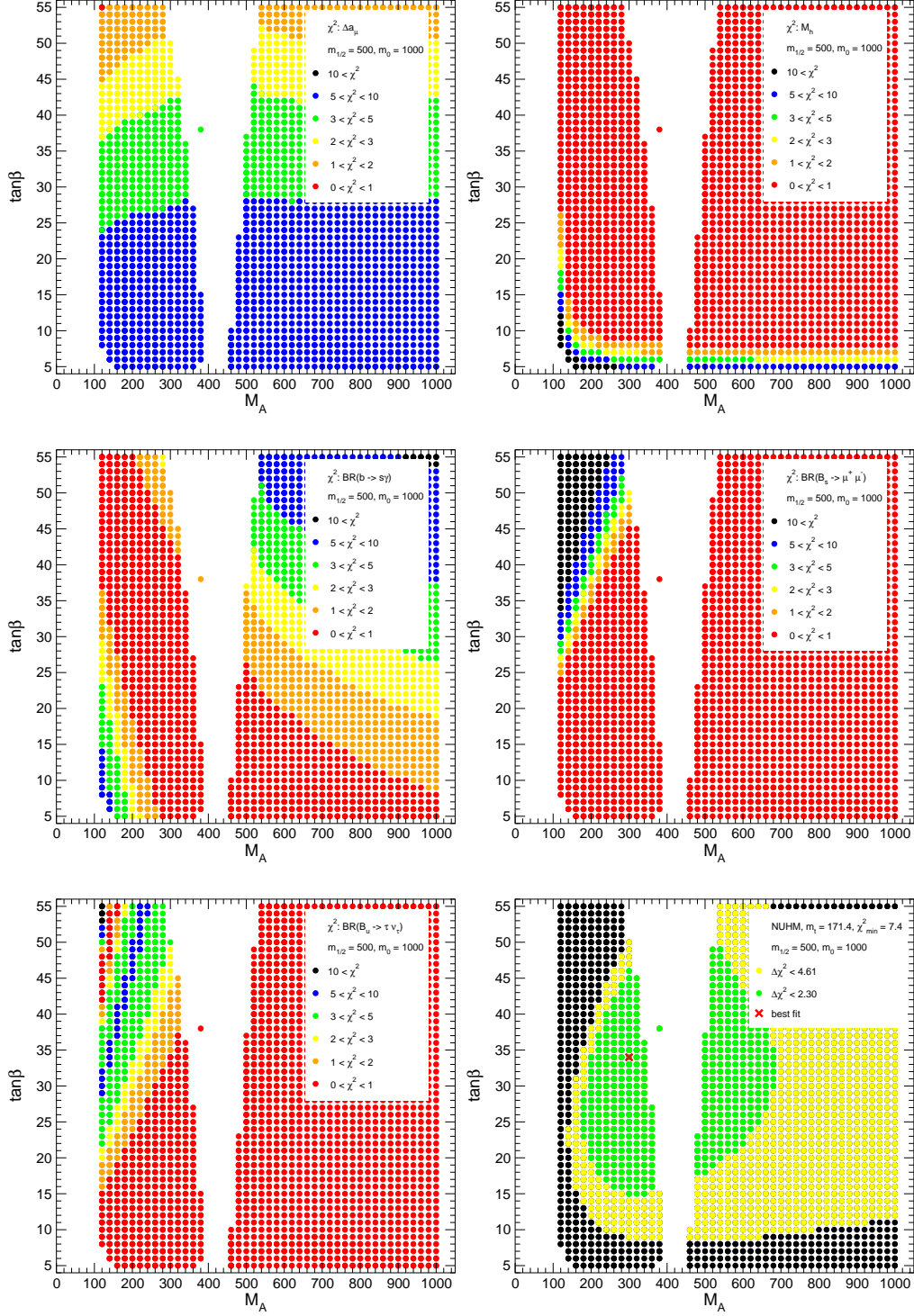


Figure 19: The most important contributions to the total χ^2 value for the NUHM ($M_A, \tan \beta$) plane **P3**, due to (a) a_μ , (b) M_h , (c) $b \rightarrow s\gamma$, (d) $B_s \rightarrow \mu^+\mu^-$ and (e) $B_u \rightarrow \tau\nu_\tau$, and (f) the combined EWPO and BPO χ^2 function. We use $m_t = 171.4 \pm 2.1$ GeV and $m_b(m_b) = 4.25 \pm 0.11$ GeV, and μ is adjusted continuously so as to yield the central value of the cold dark matter density indicated by WMAP and other observations for the central values of m_t and $m_b(m_b)$.

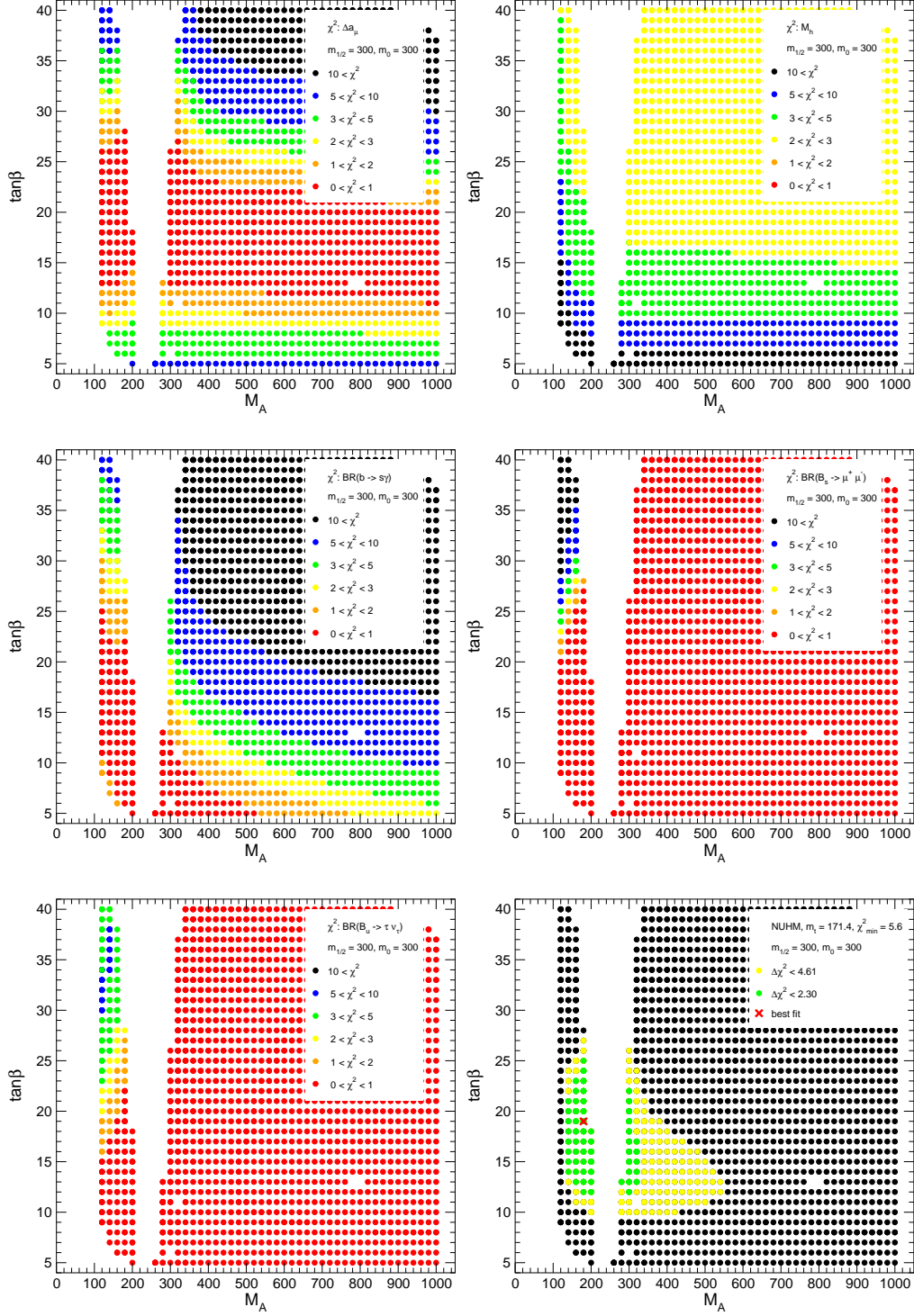


Figure 20: The most important contributions to the total χ^2 value for the NUHM1 ($M_A, \tan \beta$) plane **P4**, due to (a) a_μ , (b) M_h , (c) $b \rightarrow s\gamma$, (d) $B_s \rightarrow \mu^+\mu^-$ and (e) $B_u \rightarrow \tau\nu_\tau$, and (f) the combined EWPO and BPO χ^2 distribution. We use $m_t = 171.4 \pm 2.1$ GeV and $m_b(m_b) = 4.25 \pm 0.11$ GeV, and μ is adjusted continuously so as to yield the central value of the cold dark matter density indicated by WMAP and other observations for the central values of m_t and $m_b(m_b)$.

(most of) the NUHM parameter planes discussed above. Accordingly, for completeness we discuss the prospects for direct dark matter detection in different regions of the planes. In the cases of planes **P1** and **P2**, the direct scattering rate is generally below the CDMS upper limit [111], once one takes into account uncertainties in the strange-quark contributions to the spin-independent scattering matrix elements and in the local cold dark matter density. In the cases of plane **P3**, only in the region where M_A is small and $\tan \beta$ is high does the dark matter scattering rate approach the CDMS upper limit. However, there is a potential conflict with the preliminary XENON10 results [112] if the strange-quark contribution and/or the local relic density is large. A similar situation arises in plane **P4** for small values of M_A , almost independent of $\tan \beta$. In absence of sufficient understanding of the systematic uncertainties in the strange-quark contribution and the local cold dark matter density, we do not attempt to include the direct dark matter searches in the overall χ^2 function¹³.

The survey of NUHM parameter space made in this Section has not been exhaustive, in particular we have restricted our attention to planes with $A_0 = 0$. Nevertheless, the values of χ^2 found at the best-fit points in the various $(M_A, \tan \beta)$ planes are quite acceptable: planes **P1**, **P2**, **P3** and **P4** have $\chi^2 = 7.1, 3.5, 7.4$ and 5.6 , respectively, in fits to 9 observables with 2 free parameters in each case. It should be stressed, however, that only the **P2** plane has a minimum of χ^2 noticeably lower than that for the CMSSM fits with $\tan \beta = 10$, which occurs when $\mu = 800$ GeV, $m_0 = 300$ GeV, $M_A \sim 340$ GeV and $\tan \beta = 36$ and, moreover, at the point with the minimum value of χ^2 , the relic neutralino density is somewhat higher than the WMAP-compatible range. One might expect a greater reduction in χ^2 in a full study of the NUHM, in view of its two additional parameters compared with the CMSSM. Accordingly, we have made a preliminary study whether the quality of the NUHM fit could be improved significantly by varying A_0 , assuming the same values of m_0, M_A and $\tan \beta$ as at the best-fit point in the **P2** plane, but choosing different values of μ and $m_{1/2}$. We have investigated the possibilities $(\mu, m_{1/2}) = (800, 368)$ [**L1**], $(800, 448)$ [**L2**] and $(680, 448)$ GeV [**L3**], respectively, and varied A_0 between ± 1000 GeV. Fig. 21 shows the values of χ^2 along the lines **L1**, **L2** and **L3**. We see that the greatest improvement in χ^2 compared to the $(M_A, \tan \beta)$ planes shown previously are by ~ 0.3 only. Interestingly, the minimal values of χ^2 are found for small values of $A_0 \sim 0$. Undoubtedly some further reduction in χ^2 could be found in a more complete study, but it seems that the extra degrees of freedom in the NUHM are not crucial for the overall quality of the fit.

¹³For completeness, we note that along the WMAP strips in the CMSSM the direct dark matter scattering rate is always comfortably below the CDMS upper limit.

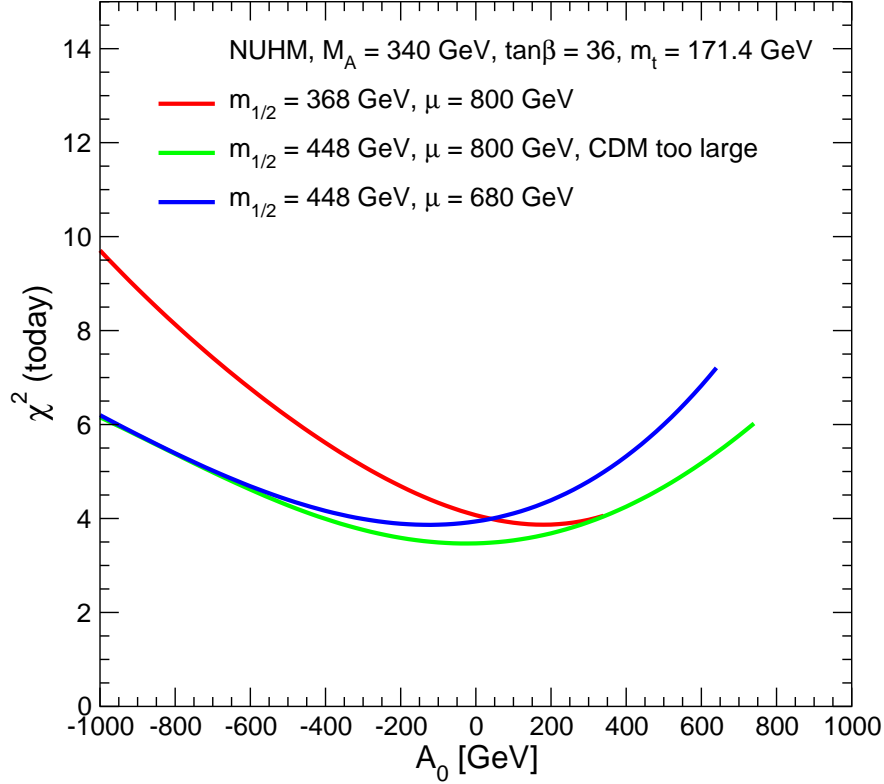


Figure 21: The dependence on A_0 of the χ^2 function along lines with $m_0 = 300$ GeV, $M_A = 340$ GeV, $\tan\beta = 36$ and $(\mu, m_{1/2}) = (800, 368)$ [L1], $(800, 448)$ [L2] and $(680, 448)$ GeV [L3], respectively.

5 Conclusions

We have analyzed previously the regions of the CMSSM parameter space preferred by the EWPO [8,9], and found a tendency to prefer regions on the WMAP coannihilation strips with relatively low values of $m_{1/2}$. These points were favoured, in particular, by the measurements of a_μ and M_W . Both these tendencies have now been reinforced, with the interpretation of a_μ based on the use of e^+e^- data to estimate the SM contribution gaining ground, and the small decrease in m_t and the slight increase in M_W tending to favour a contribution to the latter EWPO from some physics beyond the SM.

Previously, we incorporated just a single BPO into our global analysis [8,9], namely $b \rightarrow s\gamma$. Recently, data on $B_s \rightarrow \mu^+\mu^-$, $B_u \rightarrow \tau\nu_\tau$ and ΔM_{B_s} have also become available and now impinge significantly on the CMSSM parameter space. In this paper, for the first time, we have incorporated all these BPO into a global analysis.

We have found a good $\chi^2/\text{d.o.f.}$ for this global fit. However, it is clear that there is

a slight tension between the relatively low values of $m_{1/2}$ favoured by the EWPO and the absence of any corroborating indication from the BPO. Nevertheless, the global χ^2 analysis favours the appearance of relatively light sparticles that should be ‘easy’ to see at the LHC and may offer good prospects also for the ILC.

As we also have discussed here explicitly, for the first time, the global analysis strongly favours values of M_h only slightly above the lower limit established by LEP. Indeed, we find that values of $M_h < 120$ GeV are preferred, while values above 123 GeV cannot be reached in the CMSSM (for the current m_t value).

Another new step in this paper, motivated by the slight tension between the EWPO and the BPO, has been to explore the parameter space of the NUHM. We have displayed for the first time $(M_A, \tan\beta)$ planes within the NUHM over which the WMAP constraint on the cold dark matter density is generically respected. We have then shown the interplay of the various EWPO and BPO in such planes. We find that, for fixed $(m_{1/2}, m_0)$ or (m_0, μ) , relatively low values of $M_A \sim 200$ to 400 GeV are favoured, as are relatively large values of $\tan\beta \sim 20$ to 50. It is possible to find in this way NUHM points that have lower χ^2 than those possible in the CMSSM.

In the future, it will be necessary to follow closely the evolutions of both the EWPO and the BPO: improvements in the measurements of both M_W and m_t are expected, and the interpretation of a_μ may become clearer. We also expect significant improvements in the measurements of $B_s \rightarrow \mu^+\mu^-$ and $B_u \rightarrow \tau\nu_\tau$, and possibly in the interpretations of $b \rightarrow s\gamma$ and ΔM_{B_s} . The question will be whether the present slight tension between the EWPO and the BPO within the CMSSM will strengthen or relax, and a more detailed and systematic exploration of the NUHM parameter space will certainly be desirable. The implications of the EWPO and the BPO for the supersymmetric parameter space will surely be an interesting and continuing saga.

Acknowledgements

S.H. thanks C.-J. Stephen and M. Herndon for providing the χ^2 numbers for $\text{BR}(B_s \rightarrow \mu^+\mu^-)$. S.H. thanks G. Isidori and P. Paradisi about helpful communication about their analytical results for the BPO. G.W. thanks T. Becher and U. Haisch for interesting discussions. The work of K.A.O. was partially supported by DOE grant DE-FG02-94ER-40823. The work of S.H. was partially supported by CICYT (grant FPA2006-02315). Work supported in part by the European Community’s Marie-Curie Research Training Network under contract MRTN-CT-2006-035505 ‘Tools and Precision Calculations for Physics Discoveries at Colliders’

References

- [1] H. Nilles, *Phys. Rep.* **110** (1984) 1.
- [2] H. Haber and G. Kane, *Phys. Rep.* **117**, (1985) 75;
R. Barbieri, *Riv. Nuovo Cim.* **11**, (1988) 1.
- [3] Heavy Flavor Analysis group, see: <http://www.slac.stanford.edu/xorg/hfag/> .
- [4] J. Ellis, S. Kelley and D. Nanopoulos, *Phys. Lett.* **B 260** (1991) 131;
U. Amaldi, W. de Boer and H. Furstenau, *Phys. Lett.* **B 260** (1991) 447;
C. Giunti, C. Kim and U. Lee, *Mod. Phys. Lett.* **A 6** (1991) 1745.
- [5] J. Ellis, K. Olive and Y. Santoso, *Phys. Lett.* **B 539** (2002) 107, hep-ph/0204192.
- [6] J. Ellis, T. Falk, K. Olive and Y. Santoso, *Nucl. Phys.* **B 652** (2003) 259, hep-ph/0210205.
- [7] V. Berezhinsky, A. Bottino, J. Ellis, N. Fornengo, G. Mignola and S. Scopel, *Astropart. Phys.* **5** (1996) 1, hep-ph/9508249;
M. Drees, M. Nojiri, D. Roy and Y. Yamada, *Phys. Rev.* **D 56** (1997) 276, [Erratum-
ibid. **D 64** (1997) 039901], hep-ph/9701219;
M. Drees, Y. Kim, M. Nojiri, D. Toya, K. Hasuko and T. Kobayashi, *Phys. Rev.* **D 63**
(2001) 035008, hep-ph/0007202;
P. Nath and R. Arnowitt, *Phys. Rev.* **D 56** (1997) 2820, hep-ph/9701301;
A. Bottino, F. Donato, N. Fornengo and S. Scopel, *Phys. Rev.* **D 63** (2001) 125003,
hep-ph/0010203;
S. Profumo, *Phys. Rev.* **D 68** (2003) 015006, hep-ph/0304071;
D. Cerdeno and C. Munoz, *JHEP* **0410** (2004) 015, hep-ph/0405057;
H. Baer, A. Mustafayev, S. Profumo, A. Belyaev and X. Tata, *JHEP* **0507** (2005) 065,
hep-ph/0504001.
- [8] J. Ellis, S. Heinemeyer, K. Olive and G. Weiglein, *JHEP* **0502** (2005) 013, hep-ph/0411216.
- [9] J. Ellis, S. Heinemeyer, K. Olive and G. Weiglein, *JHEP* **0605** (2006) 005, hep-ph/0602220.
- [10] J. Ellis, K. Olive, Y. Santoso and V. Spanos, *Phys. Rev.* **D 69** (2004) 095004, hep-ph/0310356;

- B. Allanach and C. Lester, *Phys. Rev. D* **73** (2006) 015013, hep-ph/0507283;
 B. Allanach, *Phys. Lett. B* **635** (2006) 123, hep-ph/0601089;
 R. de Austri, R. Trotta and L. Roszkowski, *JHEP* **0605** (2006) 002, hep-ph/0602028;
JHEP **0704** (2007) 084, hep-ph/0611173; arXiv:0705.2012 [hep-ph];
 B. Allanach, C. Lester and A. M. Weber, *JHEP* **0612** (2006) 065, hep-ph/0609295;
 arXiv:0705.0487 [hep-ph].
- [11] G. Isidori, F. Mescia, P. Paradisi and D. Temes, hep-ph/0703035;
 M. Carena, A. Menon and C. Wagner, arXiv:0704.1143 [hep-ph].
- [12] J. Ellis, T. Hahn, S. Heinemeyer, K. Olive and G. Weiglein, *in preparation*.
- [13] S. Heinemeyer, W. Hollik and G. Weiglein, *Phys. Rept.* **425** (2006) 265, hep-ph/0412214.
- [14] S. Heinemeyer, W. Hollik, A.M. Weber and G. Weiglein, MPP-2007-65.
- [15] B. Allanach, G. Belanger, F. Boudjema and A. Pukhov, *JHEP* **0412** (2004) 020, hep-ph/0410091;
 H. Baer, J. Ferrandis, S. Kraml and W. Porod, *Phys. Rev. D* **73** (2006) 015010, hep-ph/0511123.
- [16] E. Brubaker et al. [Tevatron Electroweak Working Group], hep-ex/0608032, see:
<http://tevewwg.fnal.gov/top/> .
- [17] Tevatron Electroweak Working Group, hep-ex/0703034.
- [18] C. Bennett et al., *Astrophys. J. Suppl.* **148** (2003) 1, astro-ph/0302207;
 D. Spergel et al. [WMAP Collaboration], *Astrophys. J. Suppl.* **148** (2003) 175, astro-ph/0302209;
 D. Spergel et al. [WMAP Collaboration], astro-ph/0603449.
- [19] J. Ellis, K. Olive, Y. Santoso and V. Spanos, *Phys. Lett. B* **565** (2003) 176, hep-ph/0303043.
- [20] U. Chattopadhyay, A. Corsetti and P. Nath, *Phys. Rev. D* **68** (2003) 035005, hep-ph/0303201;
 H. Baer and C. Balazs, *JCAP* **0305** (2003) 006, hep-ph/0303114;
 A. Lahanas and D. Nanopoulos, *Phys. Lett. B* **568** (2003) 55, hep-ph/0303130;
 R. Arnowitt, B. Dutta and B. Hu, hep-ph/0310103.

- [21] J. Feng, K. Matchev and T. Moroi, *Phys. Rev. Lett.* **84** (2000) 2322, hep-ph/9908309;
Phys. Rev. D **61** (2000) 075005, hep-ph/9909334;
 J. Feng, K. Matchev and F. Wilczek, *Phys. Lett. B* **482** (2000) 388, hep-ph/0004043;
 J. Feng and K. Matchev, *Phys. Rev. D* **63** (2001) 095003, hep-ph/0011356.
- [22] A. Sirlin, *Phys. Rev. D* **22** (1980) 971;
 W. Marciano and A. Sirlin, *Phys. Rev. D* **22** (1980) 2695.
- [23] S. Heinemeyer, W. Hollik, D. Stöckinger, A.M. Weber and G. Weiglein, *JHEP* **08** (2006) 052, hep-ph/0604147.
- [24] P. Chankowski, A. Dabelstein, W. Hollik, W. Möhle, S. Pokorski and J. Rosiek, *Nucl. Phys. B* **417** (1994) 101.
- [25] D. Garcia and J. Solà, *Mod. Phys. Lett. A* **9** (1994) 211.
- [26] A. Djouadi, P. Gambino, S. Heinemeyer, W. Hollik, C. Jünger and G. Weiglein, *Phys. Rev. Lett.* **78** (1997) 3626, hep-ph/9612363; *Phys. Rev. D* **57** (1998) 4179, hep-ph/9710438.
- [27] S. Heinemeyer and G. Weiglein, *JHEP* **0210** (2002) 072, hep-ph/0209305; hep-ph/0301062.
- [28] J. Haestier, S. Heinemeyer, D. Stöckinger and G. Weiglein, *JHEP* **0512** (2005) 027, hep-ph/0508139; hep-ph/0506259.
- [29] The ALEPH, DELPHI, L3, OPAL, SLD Collaborations, the LEP Electroweak Working Group, the SLD Electroweak and Heavy Flavour Groups, hep-ex/0509008;
 [The ALEPH, DELPHI, L3 and OPAL Collaborations, the LEP Electroweak Working Group], hep-ex/0612034.
- [30] LEP Electroweak Working Group, see:
<http://lepewwg.web.cern.ch/LEPEWWG/Welcome.html>.
- [31] Tevatron Electroweak Working Group, see <http://tevewwg.fnal.gov> .
- [32] CDF collaboration, CDF Note 8665, see: <http://www-cdf.fnal.gov/physics/ewk/> .
- [33] M. Grünewald, private communication.
- [34] A. Czarnecki and W. Marciano, *Phys. Rev. D* **64** (2001) 013014, hep-ph/0102122.

- [35] M. Knecht, *Lect. Notes Phys.* **629** (2004) 37, hep-ph/0307239;
M. Passera, *Nucl. Phys. Proc. Suppl.* **155** (2006) 365, hep-ph/0509372.
- [36] D. Stöckinger, *J. Phys. G* **34** (2007) R45, hep-ph/0609168.
- [37] J. Miller, E. de Rafael and B. Roberts, hep-ph/0703049.
- [38] F. Jegerlehner, hep-ph/0703125.
- [39] T. Kinoshita and M. Nio, *Phys. Rev. D* **70** (2004) 113001, hep-ph/0402206; *Phys. Rev.* **73** (2006) 053007, hep-ph/0512330.
- [40] M. Passera, *Phys. Rev. D* **75** (2007) 013002, hep-ph/0606174.
- [41] M. Davier, S. Eidelman, A. Höcker and Z. Zhang, *Eur. Phys. J. C* **31** (2003) 503, hep-ph/0308213.
- [42] K. Hagiwara, A. Martin, D. Nomura and T. Teubner, *Phys. Rev. D* **69** (2004) 093003, hep-ph/0312250.
- [43] K. Hagiwara, A. Martin, D. Nomura and T. Teubner, *Phys. Lett. B* **649** (2007) 173, hep-ph/0611102.
- [44] S. Ghozzi and F. Jegerlehner, *Phys. Lett. B* **583** (2004) 222, hep-ph/0310181.
- [45] J. de Troconiz and F. Yndurain, *Phys. Rev. D* **71** (2005) 073008, hep-ph/0402285.
- [46] M. Davier, hep-ph/0701163.
- [47] J. Bijnens, E. Pallante and J. Prades, *Phys. Rev. Lett.* **75** (1995) 1447 [Erratum-ibid. **75** (1995) 3781], hep-ph/9505251; *Nucl. Phys. B* **474** (1996) 379, hep-ph/9511388; *Nucl. Phys. B* **626** (2002) 410, hep-ph/0112255.
- [48] M. Hayakawa, T. Kinoshita and A. Sanda, *Phys. Rev. D* **54** (1996) 3137, hep-ph/9601310;
M. Hayakawa and T. Kinoshita, *Phys. Rev. D* **57** (1998) 465 [Erratum-ibid. **D 66** (2002) 019902], hep-ph/9708227; hep-ph/0112102.
- [49] M. Knecht and A. Nyffeler, *Phys. Rev. D* **65** (2002) 073034, hep-ph/0111058;
M. Knecht, A. Nyffeler, M. Perrottet and E. De Rafael, *Phys. Rev. Lett.* **88** (2002) 071802, hep-ph/0111059;

- I. Blokland, A. Czarnecki and K. Melnikov, *Phys. Rev. Lett.* **88** (2002) 071803, hep-ph/0112117;
M. Ramsey-Musolf and M. Wise, *Phys. Rev. Lett.* **89** (2002) 041601, hep-ph/0201297;
J. Kühn, A. Onishchenko, A. Pivovarov and O. Veretin, *Phys. Rev. D* **68** (2003) 033018, hep-ph/0301151.
- [50] K. Melnikov and A. Vainshtein, *Phys. Rev. D* **70** (2004) 113006, hep-ph/0312226.
- [51] M. Davier and W. Marciano, *Ann. Rev. Nucl. Part. Sci.* **54** (2004) 115.
- [52] A. Aloisio et al. [KLOE Collaboration], *Phys. Lett.* **606** (2005) 12, hep-ex/0407048;
D. Leone [KLOE Collaboration], *Nucl. Phys. Proc. Suppl.* **162** (2006) 95.
- [53] R. Akhmetshin et al. [CMD-2 Collaboration], *Phys. Lett. B* **578** (2004) 285, hep-ex/0308008; hep-ex/0610021.
- [54] M. Achasov et al. [SND Collaboration], *J. Exp. Theor. Phys.* **101** (2005) 1053, hep-ex/0506076.
- [55] G. Bennett et al. [The Muon g-2 Collaboration], *Phys. Rev. Lett.* **92** (2004) 161802, hep-ex/0401008.
- [56] G. Bennett et al. [The Muon g-2 Collaboration], *Phys. Rev. D* **73** (2006) 072003, hep-ex/0602035.
- [57] S. Eidelman, talk given at the ICHEP06, Moscow, July 2006, see:
http://ichep06.jinr.ru/reports/333_6s1_9p30_Eidelman.pdf .
- [58] T. Moroi, *Phys. Rev. D* **53** (1996) 6565 [Erratum-ibid. **D 56** (1997) 4424], hep-ph/9512396.
- [59] J. Lopez, D. Nanopoulos and X. Wang, *Phys. Rev. D* **49** (1994) 366; hep-ph/9308336;
U. Chattopadhyay and P. Nath, *Phys. Rev. D* **53** (1996) 1648, hep-ph/9507386.
- [60] G. Degrossi and G. Giudice, *Phys. Rev. D* **58** (1998) 053007, hep-ph/9803384.
- [61] S. Heinemeyer, D. Stöckinger and G. Weiglein, *Nucl. Phys. B* **690** (2004) 62, hep-ph/0312264.
- [62] S. Heinemeyer, D. Stöckinger and G. Weiglein, *Nucl. Phys. B* **699** (2004) 103, hep-ph/0405255.

- [63] S. Heinemeyer, W. Hollik and G. Weiglein, *Comp. Phys. Commun.* **124** 2000 76, hep-ph/9812320. The code is accessible via <http://www.feynhiggs.de>.
- [64] S. Heinemeyer, W. Hollik and G. Weiglein, *Eur. Phys. J.* **C 9** (1999) 343, hep-ph/9812472.
- [65] M. Frank, T. Hahn, S. Heinemeyer, W. Hollik, H. Rzehak and G. Weiglein, *JHEP* **02** (2007) 047, hep-ph/0611326.
- [66] Y. Okada, M. Yamaguchi, T. Yanagida, *Prog. Theor. Phys.* **85** (1991) 1;
J. Ellis, G. Ridolfi, F. Zwirner, *Phys. Lett.* **B 257** (1991) 83;
H. Haber, R. Hempfling, *Phys. Rev. Lett.* **66** (1991) 1815.
- [67] P. Chankowski, S. Pokorski, J. Rosiek, *Phys. Lett.* **B 286** (1992) 307; *Nucl. Phys.* **B 423** (1994) 437, hep-ph/9303309.
- [68] A. Dabelstein, *Nucl. Phys.* **B 456** (1995) 25, hep-ph/9503443; *Z. Phys.* **C 67** (1995) 495, hep-ph/9409375.
- [69] G. Degrandi, S. Heinemeyer, W. Hollik, P. Slavich, G. Weiglein, *Eur. Phys. J.* **C 28** (2003) 133, hep-ph/0212020.
- [70] M. Carena, D. Garcia, U. Nierste and C. Wagner, *Nucl. Phys.* **B 577** (2000) 577, hep-ph/9912516;
H. Eberl, K. Hidaka, S. Kraml, W. Majerotto and Y. Yamada, *Phys. Rev.* **D 62** (2000) 055006, hep-ph/9912463.
- [71] T. Banks, *Nucl. Phys.* **B 303** (1988) 172;
L. Hall, R. Rattazzi and U. Sarid, *Phys. Rev.* **D 50** (1994) 7048, hep-ph/9306309;
R. Hempfling, *Phys. Rev.* **D 49** (1994) 6168;
M. Carena, M. Olechowski, S. Pokorski and C. Wagner, *Nucl. Phys.* **B 426** (1994) 269, hep-ph/9402253.
- [72] G. Degrandi, A. Dedes, P. Slavich, *Nucl. Phys.* **B 672** (2003) 144, hep-ph/0305127.
- [73] S. Martin, *Phys. Rev.* **D 65** (2002) 116003, hep-ph/0111209; *Phys. Rev.* **D 66** (2002) 096001, hep-ph/0206136; *Phys. Rev.* **D 67** (2003) 095012, hep-ph/0211366; *Phys. Rev.* **D 68** 075002 (2003), hep-ph/0307101; *Phys. Rev.* **D 70** (2004) 016005, hep-ph/0312092; *Phys. Rev.* **D 71** (2005) 016012, hep-ph/0405022; *Phys. Rev.* **D 71** (2005) 116004, hep-ph/0502168;

- S. Martin and D. Robertson, *Comput. Phys. Commun.* **174** (2006) 133, hep-ph/0501132.
- [74] S. Martin, *Phys. Rev. D* **75** (2007) 055005, hep-ph/0701051.
- [75] S. Heinemeyer, W. Hollik, H. Rzehak and G. Weiglein, *Eur. Phys. J. C* **39** (2005) 465, hep-ph/0411114; hep-ph/0506254.
- [76] B. Allanach, A. Djouadi, J. Kneur, W. Porod and P. Slavich, *JHEP* **0409** (2004) 044, hep-ph/0406166.
- [77] LEP Higgs working group, *Eur. Phys. J. C* **47** (2006) 547, hep-ex/0602042.
- [78] LEP Higgs working group, *Phys. Lett. B* **565** (2003) 61, hep-ex/0306033.
- [79] S. Ambrosanio, A. Dedes, S. Heinemeyer, S. Su and G. Weiglein, *Nucl. Phys. B* **624** (2001) 3, hep-ph/0106255.
- [80] J. Ellis, S. Heinemeyer, K. Olive and G. Weiglein, *Phys. Lett. B* **515** (2001) 348, hep-ph/0105061.
- [81] W. Yao et al. [Particle Data Group Collaboration], *J. Phys. G* **33** (2006) 1.
- [82] M. Misiak et al., *Phys. Rev. Lett.* **98** (2007) 022002, hep-ph/0609232.
- [83] T. Hurth, E. Lunghi and W. Porod, *Nucl. Phys. B* **704** (2005) 56, hep-ph/0312260.
- [84] M. Neubert, *Eur. Phys. J. C* **40** (2005) 165, hep-ph/0408179.
- [85] R. Barate et al. [ALEPH Collaboration], *Phys. Lett. B* **429** (1998) 169;
S. Chen et al. [CLEO Collaboration], *Phys. Rev. Lett.* **87** (2001) 251807, hep-ex/0108032;
P. Koppenburg et al. [Belle Collaboration], *Phys. Rev. Lett.* **93** (2004) 061803, hep-ex/0403004;
K. Abe et al. [Belle Collaboration], *Phys. Lett. B* **511** (2001) 151, hep-ex/0103042;
B. Aubert et al. [BABAR Collaboration], hep-ex/0207074; hep-ex/0207076.
- [86] K. Adel and Y. Yao, *Phys. Rev. D* **49** (1994) 4945, hep-ph/9308349;
C. Greub, T. Hurth and D. Wyler, *Phys. Lett. B* **380** (1996) 385, hep-ph/9602281;
Phys. Rev. D **54** (1996) 3350, hep-ph/9603404;
A. Ali, talk given at ICHEP04, Beijing, August 2004, appeared in the proceedings, see: <http://ichep04.ihep.ac.cn/db/paper.php> .

- [87] K. Chetyrkin, M. Misiak and M. Münz, *Phys. Lett. B* **400**, (1997) 206 [Erratum-ibid. **B 425** (1998) 414], hep-ph/9612313.
- [88] P. Cho, M. Misiak and D. Wyler, *Phys. Rev. D* **54**, 3329 (1996), hep-ph/9601360;
A. Kagan and M. Neubert, *Eur. Phys. J. C* **7** (1999) 5, hep-ph/9805303;
A. Ali, E. Lunghi, C. Greub and G. Hiller, *Phys. Rev. D* **66** (2002) 034002, hep-ph/0112300;
G. Hiller and F. Krüger, *Phys. Rev. D* **69** (2004) 074020, hep-ph/0310219;
M. Carena, D. Garcia, U. Nierste and C. Wagner, *Phys. Lett. B* **499** (2001) 141, hep-ph/0010003;
D. Demir and K. Olive, *Phys. Rev. D* **65** (2002) 034007, hep-ph/0107329;
T. Hurth, hep-ph/0212304.
- [89] P. Gambino and M. Misiak, *Nucl. Phys. B* **611** (2001) 338, hep-ph/0104034.
- [90] G. Belanger, F. Boudjema, A. Pukhov and A. Semenov, *Comput. Phys. Commun.* **149** (2002) 103, hep-ph/0112278; hep-ph/0405253.
- [91] C. Degrandi, P. Gambino and G. Giudice, *JHEP* **0012** (2000) 009, hep-ph/0009337.
- [92] G. Buchalla and A. Buras, *Nucl. Phys. B* **400** (1993) 225;
M. Misiak and J. Urban, *Phys. Lett. B* **451** (1999) 161, hep-ph/9901278;
G. Buchalla and A. Buras, *Nucl. Phys. B* **548** (1999) 309, hep-ph/9901288;
A. Buras, *Phys. Lett. B* **566** (2003) 115, hep-ph/0303060.
- [93] CDF Collaboration, CDF Public Note 8176, see:
<http://www-cdf.fnal.gov/physics/new/bottom/060316.blessed-bsmumu3/> .
- [94] D0 Collaboration, D0 Note 5344-Conf, see:
<http://www-d0.fnal.gov/Run2Physics/WWW/results/b.htm> .
- [95] CDF Collaboration, see: <http://www-cdf.fnal.gov/physics/projections/> .
- [96] P. Ball et al., hep-ph/0003238.
- [97] K. Babu and C. Kolda, *Phys. Rev. Lett.* **84** (2000) 228, hep-ph/9909476;
S. Choudhury and N. Gaur, *Phys. Lett. B* **451** (1999) 86, hep-ph/9810307;
C. Bobeth, T. Ewerth, F. Krüger and J. Urban, *Phys. Rev. D* **64** (2001) 074014, hep-ph/0104284;

- A. Dedes, H. Dreiner and U. Nierste, *Phys. Rev. Lett.* **87** (2001) 251804, hep-ph/0108037;
 G. Isidori and A. Retico, *JHEP* **0111** (2001) 001, hep-ph/0110121;
 A. Dedes and A. Pilaftsis, *Phys. Rev. D* **67** (2003) 015012, hep-ph/0209306;
 A. Buras, P. Chankowski, J. Rosiek and L. Slawianowska, *Nucl. Phys. B* **659** (2003) 3, hep-ph/0210145;
 A. Dedes, *Mod. Phys. Lett. A* **18** (2003) 2627, hep-ph/0309233.
- [98] J. Ellis, K. Olive and V. Spanos, *Phys. Lett. B* **624** (2005) 47, hep-ph/0504196.
- [99] C. Bernard, *Nucl. Phys. Proc. Suppl.* **94** (2001) 159, hep-lat/0011064;
 M. Wingate, C. Davies, A. Gray, G. Lepage and J. Shigemitsu, *Phys. Rev. Lett.* **92** (2004) 162001, hep-ph/0311130.
- [100] K. Ikado et al. [Belle Collaboration], hep-ex/0604018.
- [101] B. Aubert et al. [BABAR Collaboration], hep-ex/0608019.
- [102] G. Isidori and P. Paradisi, *Phys. Lett. B* **639** (2006) 499, hep-ph/0605012.
- [103] A. Abulencia et al. [CDF Collaboration], *Phys. Rev. Lett.* **97** (2006) 062003, hep-ex/0606027.
- [104] V. Abazov et al. [D0 Collaboration], *Phys. Rev. Lett.* **97** (2006) 021802, hep-ex/0603029.
- [105] G. Isidori and A. Retico, *JHEP* **0111** (2001) 001, hep-ph/0110121;
 A. Buras, P. Chankowski, J. Rosiek and L. Slawianowska, *Nucl. Phys. B* **619** (2001) 434, hep-ph/0107048; *Phys. Lett. B* **546** (2002) 96, hep-ph/0207241; *Nucl. Phys. B* **659** (2003) 3, hep-ph/0210145;
 G. D'Ambrosio, G. Giudice, G. Isidori and A. Strumia, *Nucl. Phys. B* **645** (2002) 155, hep-ph/0207036.
- [106] M. Bona et al. [UTfit Collaboration], *JHEP* **0603** (2006) 080, hep-ph/0509219.
- [107] J. Ellis, S. Heinemeyer, K. Olive and G. Weiglein, *JHEP* **0301** (2003) 006, hep-ph/0211206.
- [108] M. Carena, S. Heinemeyer, C. Wagner and G. Weiglein, hep-ph/9912223.

- [109] M. Carena, S. Heinemeyer, C. Wagner and G. Weiglein, *Eur. Phys. J. C* **26** (2003) 601, hep-ph/0202167.
- [110] M. Carena, S. Heinemeyer, C. Wagner and G. Weiglein, *Eur. Phys. J. C* **45** (2006) 797, hep-ph/0511023.
- [111] D. Akerib et al. [CDMS Collaboration], *Phys. Rev. Lett.* **96** (2006) 011302, astro-ph/0509259.
- [112] J. Angle et al. [XENON10 Collaboration], arXiv:0706.0039 [astro-ph],
see also: <http://xenon.astro.columbia.edu/> .